

Thermal versus entropic Mpemba effect in molecular gases with nonlinear drag

Alberto Megías*

Departamento de Física, Universidad de Extremadura, E-06006 Badajoz, Spain

Andrés Santos†

*Departamento de Física, Universidad de Extremadura, E-06006 Badajoz, Spain and
Instituto de Computación Científica Avanzada (ICCAEx),
Universidad de Extremadura, E-06006 Badajoz, Spain*

Antonio Prados‡

Física Teórica, Universidad de Sevilla, Apartado de Correos 1065, E-41080 Sevilla, Spain

(Dated: February 1, 2022)

Loosely speaking, the Mpemba effect appears when the hotter cools sooner or, in a more abstract way, when the further from equilibrium relaxes faster. In this paper, we investigate the Mpemba effect in a molecular gas with nonlinear drag, both analytically—by employing the tools of kinetic theory—and numerically—direct simulation Monte Carlo of the kinetic equation and event-driven molecular dynamics. The Mpemba effect is analyzed via two alternative routes, recently considered in the literature. First, the kinetic or thermal route, in which the emergence of the Mpemba effect is marked by the crossing of the evolution curves of the kinetic temperature (average kinetic energy). Second, the stochastic thermodynamics or entropic route, in which the emergence of the Mpemba effect is marked by the crossing of the distance to equilibrium in probability space. A nonmutual correspondence between the thermal and entropic Mpemba effects is found in a certain region of parameters. Our theoretical description, which involves an extended Sonine approximation in which not only the excess kurtosis but also the sixth cumulant is retained, gives an excellent account of the behavior observed in simulations.

NOMENCLATURE

Acronyms

AGF	Approximate Green function
BSA	Basic Sonine approximation
DSMC	Direct simulation Monte Carlo
ESA	Extended Sonine approximation
EDMD	Event-driven molecular dynamics
EFPE	Enskog–Fokker–Planck equation
EME	Entropic Mpemba effect
KIME	Kovacs-induced Mpemba effect
KLD	Kullback–Leibler divergence
LBSA	Linearized basic Sonine approximation
LE	Local equilibrium
ME	Mpemba effect
TME	Thermal Mpemba effect
VDF	Velocity distribution function

I. INTRODUCTION

In recent years, memory effects have become a hot topic in nonequilibrium statistical physics research [1]. Those phenomena usually imply counterintuitive effects that apparently contradict well-established stan-

dard physical laws. One of the most interesting is the Mpemba effect (ME): given two samples of a fluid in a common thermal bath, the initially hotter one may cool more rapidly than that initially cooler. Well-known Newton’s law of cooling, according to which the temperature evolution is predetermined by its initial value, is thus violated in the presence of the ME. Original studies of the ME deal with water [2–32], and even today there is still a lack of consensus about its existence in this very complex system [33–35].

In a more general context, the ME can be recast as “the initially further from equilibrium relaxes faster”—with the separation from equilibrium being defined in a suitable way, see below. With such an interpretation, Mpemba-like effects have been investigated in a large variety of many-body systems: molecular gases [36, 37], mixtures [38], granular gases [39–44], inertial suspensions [45, 46], spin glasses [47], carbon nanotube resonators [48], clathrate hydrates [49], Markovian models [50–54], active systems [55], Ising models [56, 57], non-Markovian mean-field systems [58, 59], or quantum systems [60]. Also, it has been experimentally observed in colloids [61, 62].

There have been two main approaches to the ME: the kinetic-theory or “thermal” approach [36–46] and the stochastic-process (or thermodynamics) or “entropic” approach [50–55, 60–62]. In the thermal approach, kinetic theory makes it possible to define in a natural way an out-of-equilibrium time-dependent temperature $T(t)$ (basically, the average kinetic energy). This allows for a simple, and close in spirit to the original studies in water,

* albertom@unex.es

† andres@unex.es

‡ prados@us.es

characterization of the separation from equilibrium (at temperature T_{eq}): the initially hotter (colder) sample A (B) translates into that having the larger (smaller) initial value of the kinetic temperature, $T_A^0 > T_B^0 > T_{\text{eq}}$. The *thermal* Mpemba effect (TME) emerges when the evolution curves for the temperature cross at a certain time t_θ , $T_A(t_\theta) = T_B(t_\theta)$, and that of the initially hotter remains below the other one for longer times, $T_{\text{eq}} < T_A(t) < T_B(t)$ for $t > t_\theta$.

In the stochastic-process approach, the starting point is usually a Markov process $\mathbf{x}(t)$. The state of the system at time t is determined by a probability distribution $P(\mathbf{x}, t)$, which typically obeys a master equation (for discrete \mathbf{x}) or a Fokker–Planck equation (for continuous $\mathbf{x}(t)$). At equilibrium, the probability distribution is $P_{\text{eq}}(\mathbf{x})$, and the Kullback–Leibler divergence (KLD) or relative entropy [63] is defined as

$$\mathcal{D}(t) \equiv \left\langle \ln \frac{P}{P_{\text{eq}}} \right\rangle = \int d\mathbf{x} P(\mathbf{x}, t) \ln \frac{P(\mathbf{x}, t)}{P_{\text{eq}}(\mathbf{x})}. \quad (1)$$

The H -theorem [64] ensures that $\mathcal{D}(t)$ monotonically decreases to zero over a nonequilibrium process and thus $\mathcal{D}(t)$ can be interpreted as the “distance” to equilibrium from a physical standpoint [65]. Also, \mathcal{D} can be understood as (the opposite of) the nonequilibrium entropy relative to the equilibrium state. The ME is translated as follows in this context: the further from (closer to) sample A (B) has the larger (smaller) initial value of \mathcal{D} , i.e., $\mathcal{D}_A^0 > \mathcal{D}_B^0 > 0$. The *entropic* Mpemba effect (EME) emerges when the evolution curves for \mathcal{D} cross at a certain time $t_{\mathcal{D}}$, $\mathcal{D}_A(t_{\mathcal{D}}) = \mathcal{D}_B(t_{\mathcal{D}})$, and $0 < \mathcal{D}_A(t) < \mathcal{D}_B(t)$ for $t > t_{\mathcal{D}}$.

It is clear that the two effects described above, TME and EME, are equivalent if a biunivocal correspondence between nonequilibrium temperature and entropy exists. Still, this is not the case in general, as we will show. In fact, the main aim of this paper is to analyze the correspondence between the TME and the EME in a prototypical system, where the two approaches can be carried out analytically—at least in an approximate, systematic, way. Specifically, we consider a molecular gas of hard particles that is coupled to a thermal bath, with the resulting drag force being nonlinear in the velocity [36]. To that end, we will use kinetic-theory tools (via a Sonine approximation of the Boltzmann equation) in combination with direct simulation Monte Carlo (DSMC) and event-driven molecular dynamics (EDMD) simulations.

Let us consider the following model for a fluid with nonlinear drag [36, 37, 66–68]: a d -dimensional fluid of elastic hard spheres of mass m and diameter σ , with number density n , subjected to a stochastic force composed by a white-noise term with nonlinear variance plus a nonlinear drag force. This scheme mimics a system of elastic spheres assumed to be suspended in a background fluid in equilibrium at temperature T_b . The (spatially uniform) Enskog–Fokker–Planck equation (EFPE) of the one-body

velocity distribution function (VDF) $f(\mathbf{v}, t)$ reads

$$\partial_t f(\mathbf{v}, t) - \frac{\partial}{\partial \mathbf{v}} \cdot \left[\zeta(v) \mathbf{v} + \frac{\xi^2(v)}{2} \right] f(\mathbf{v}, t) = J[\mathbf{v}|f, f], \quad (2)$$

where

$$J[\mathbf{v}_1|f, f] = \sigma^{d-1} g_c \int d\mathbf{v}_2 \int_+ d\hat{\boldsymbol{\sigma}} \mathbf{v}_{12} \cdot \hat{\boldsymbol{\sigma}} \times [f(\mathbf{v}'_1, t) f(\mathbf{v}'_2, t) - f(\mathbf{v}_1, t) f(\mathbf{v}_2, t)] \quad (3)$$

is the usual Boltzmann–Enskog collision operator with $\mathbf{v}_{12} \equiv \mathbf{v}_1 - \mathbf{v}_2$, $g_c = \lim_{r \rightarrow \sigma^+} g(r)$ being the contact value of the pair correlation function, and $\int_+ d\hat{\boldsymbol{\sigma}} \equiv \int d\hat{\boldsymbol{\sigma}} \Theta(\mathbf{v}_{12} \cdot \hat{\boldsymbol{\sigma}})$. In addition, the drag component of the stochastic force is $-m\zeta(v)\mathbf{v}$, while the white-noise counterpart has a non-linear variance $m^2\xi^2(v)$. The functions $\zeta(v)$ and $\xi^2(v)$ are connected via the fluctuation-dissipation theorem as

$$\xi^2(v) = \frac{2k_B T_b}{m} \zeta(v), \quad (4)$$

where k_B is the Boltzmann constant and T_b is the temperature of the background fluid. This ensures that the only stationary solution of the EFPE is the equilibrium Maxwellian,

$$f^{\text{eq}}(\mathbf{v}) = n \left(\frac{m}{2\pi k_B T_b} \right)^{d/2} e^{-mv^2/2k_B T_b}. \quad (5)$$

A quadratic dependence of the drag coefficient naturally appears when the hard spheres and the background fluid particles have a comparable mass [36, 37, 66–68],

$$\zeta(v) = \zeta_0 \left(1 + \gamma \frac{mv^2}{k_B T_b} \right). \quad (6)$$

The coefficients ζ_0 and γ are both positive and measure the zero-velocity value and the degree of nonlinearity, respectively, of the drag coefficient $\zeta(v)$. Note that, due to the nonlinearity of the drag coefficient $\zeta(v)$, the implementation of the Langevin equation associated with the EFPE, Eq. (2), is far from trivial. This issue is discussed in Appendix A.

The two approaches to the ME can be implemented in the nonlinear fluid introduced above. On the one hand, the nonequilibrium temperature $T(t)$ is defined as usual,

$$\frac{d}{2} k_B T(t) = \frac{m}{2} \langle v^2 \rangle = \frac{m}{2n} \int d\mathbf{v} v^2 f(\mathbf{v}, t), \quad (7)$$

where

$$n = \int d\mathbf{v} f(\mathbf{v}, t) \quad (8)$$

is the number density. On the other hand, the relative entropy is introduced in the kinetic approach as

$$\mathcal{D}(t) = \left\langle \ln \frac{f}{f_{\text{eq}}} \right\rangle = \frac{1}{n} \int d\mathbf{v} f(\mathbf{v}, t) \ln \frac{f(\mathbf{v}, t)}{f^{\text{eq}}(\mathbf{v})}. \quad (9)$$

The factor $1/n$ is due to the normalization of the VDF, Eq. (8).

With the above definitions, both the TME and the EME can be investigated. Some basic questions arise, though. Does the TME imply the EME, or vice versa? When both of them are present, how close are the respective crossover times t_θ and $t_{\mathcal{D}}$? Is it possible to observe the ME if the temperature of at least one of the two samples overshoots its equilibrium value?

On physical grounds, it is expected that the evolution of the gas toward equilibrium takes place along two stages [69]. First, a rapid “kinetic” stage where the VDF approaches the so-called local equilibrium (LE) form,

$$f^{\text{LE}}(\mathbf{v}; T(t)) = n \left[\frac{m}{2\pi k_B T(t)} \right]^{d/2} e^{-mv^2/2k_B T(t)}, \quad (10)$$

i.e., f^{LE} has the Maxwellian shape but with the time-dependent temperature. Second, a slower “hydrodynamic” stage, where the VDF is close to f^{LE} and the evolution of the VDF takes place via the temperature.

The above discussion suggests the following decomposition for the relative entropy,

$$\mathcal{D}(t) = \mathcal{D}^{\text{kin}}(t) + \mathcal{D}^{\text{LE}}(T(t)), \quad (11)$$

where

$$\mathcal{D}^{\text{kin}}(t) = \frac{1}{n} \int d\mathbf{v} f(\mathbf{v}, t) \ln \frac{f(\mathbf{v}, t)}{f^{\text{LE}}(\mathbf{v}; T(t))} \quad (12a)$$

and

$$\begin{aligned} \mathcal{D}^{\text{LE}}(T(t)) &= \frac{1}{n} \int d\mathbf{v} f(\mathbf{v}, t) \ln \frac{f^{\text{LE}}(\mathbf{v}; T(t))}{f^{\text{eq}}(\mathbf{v})} \\ &= \frac{1}{n} \int d\mathbf{v} f^{\text{LE}}(\mathbf{v}; T(t)) \ln \frac{f^{\text{LE}}(\mathbf{v}; T(t))}{f^{\text{eq}}(\mathbf{v})} \\ &= \frac{d}{2} [\theta(t) - 1 - \ln \theta(t)], \quad \theta(t) \equiv \frac{T(t)}{T_b}. \end{aligned} \quad (12b)$$

Both \mathcal{D}^{kin} and \mathcal{D}^{LE} are positive definite [70]. The first contribution \mathcal{D}^{kin} is a measure of the departure of the true VDF from the LE one, and depends explicitly on time through the whole VDF $f(\mathbf{v}, t)$. In contrast, the second contribution \mathcal{D}^{LE} measures the deviation of the LE state from the asymptotic equilibrium state and only depends on time through the nonequilibrium temperature $T(t)$, namely on the temperature ratio $\theta(t)$. More specifically, \mathcal{D}^{LE} monotonically increases as $|\theta - 1|$ increases in the domains $\theta > 1$ and $\theta < 1$ separately.

The TME and EME can be directly related if the crossing comes about in the hydrodynamic regime, since therein $\mathcal{D}^{\text{kin}} \approx 0$ and $\mathcal{D}(t) \approx \mathcal{D}^{\text{LE}}(\theta(t))$ —which is a function of temperature only, as explicitly stated by our notation. Therefore, the TME and EME become equivalent during the hydrodynamic stage, and $t_\theta \simeq t_{\mathcal{D}}$. However, we will show that in most situations the ME occurs during the kinetic stage, the contribution \mathcal{D}^{kin} is then relevant, and the physical picture is much more complex.

In fact, the two-stage relaxation picture may even break down under certain conditions, as discussed in Ref. [71].

The paper is organized as follows. In Sec. II, we derive the evolution equations for the relevant physical quantities, within the Sonine approximation schemes developed in this paper. From this knowledge, the general phenomenology of TME and EME is predicted and described from heuristic arguments in Sec. III. Afterwards, in Sec. IV a singular case for TME, induced by the appearance of a Kovacs-like effect, is discussed. We present simulation results supporting the theoretical predictions in Sec. V. Finally, conclusions are presented in Sec. VI. Some of the technical parts are relegated to the Appendices.

II. EVOLUTION EQUATIONS

Multiplying both sides of Eq. (2) by v^2 and integrating over velocity one readily obtains the evolution equation for the time-dependent temperature,

$$\frac{\dot{T}}{\zeta_0} = -2(T - T_b) \left[1 + (d+2)\gamma \frac{T}{T_b} \right] - 2(d+2)\gamma \frac{T^2}{T_b} a_2, \quad (13)$$

where

$$a_2(t) = \frac{d}{d+2} \frac{\langle v^4 \rangle}{\langle v^2 \rangle^2} - 1 \quad (14)$$

is the excess kurtosis.

Notice that one gets Newton’s cooling law $\dot{T} = -2\zeta_0(T - T_b)$ in the linear case $\gamma = 0$. However, if $\gamma \neq 0$, the evolution of temperature is coupled to that of the fourth-degree moment $\langle v^4 \rangle$ through a_2 . Next, the evolution equation for $\langle v^4 \rangle$ stemming from the EFPE, Eq. (2), is coupled to the sixth-degree moment $\langle v^6 \rangle$ due to the nonlinear drag term and to all the moments $\langle v^\ell \rangle$ due to the collision term, and so on. Thus, the full evolution of $T(t)$ is coupled to the infinite hierarchy of moment equations.

To write the hierarchy of moment equations, it is convenient to introduce dimensionless quantities [36]. First, we define a rescaled velocity \mathbf{c} as

$$\mathbf{c} \equiv \frac{\mathbf{v}}{v_{\text{th}}(t)}, \quad v_{\text{th}}(t) \equiv \sqrt{\frac{2k_B T(t)}{m}}, \quad (15)$$

in which $v_{\text{th}}(t)$ is the thermal velocity at time t . Analogously, the dimensionless VDF is introduced as

$$\phi(\mathbf{c}, t) \equiv \frac{v_{\text{th}}^d(t)}{n} f(\mathbf{v}, t). \quad (16)$$

Using as unit of time the mean free time—average time between collisions—at equilibrium,

$$\tau_b = \frac{K_d}{g_c n \sigma^{d-1} \sqrt{2k_B T_b/m}}, \quad K_d \equiv \frac{\sqrt{2}\Gamma(d/2)}{\pi^{\frac{d-1}{2}}}, \quad (17)$$

the dimensionless time t^* and zero-velocity drag coefficient ζ_0^* can be defined as

$$t^* = \frac{t}{\tau_b}, \quad \zeta_0^* = \zeta_0 \tau_b. \quad (18)$$

The parameter ζ_0^* measures the relative relevance of the drag force (i.e., the interactions between the particles and the background fluid) and hard-sphere binary collisions. The limit $\zeta_0^* \rightarrow 0$ corresponds to negligible drag force, where the EFPE reduces to the Enskog equation. The limit $\zeta_0^* \rightarrow \infty$ corresponds to negligible collisions, where the EFPE reduces to the Fokker–Planck equation [72]. In this work, we typically consider the value $\zeta_0^* = 1$, for which the drag force and binary collisions are comparable and act over the same time scale. Note that both the drag force and binary collisions drive by themselves the system to equilibrium, independently of the magnitude of the other interaction, with the entropic distance monotonically decreasing to zero [73].

In terms of these reduced quantities, the EFPE, Eq. (2), can be rewritten as

$$\partial_t \phi(\mathbf{c}, t) = \frac{1}{2\theta} \partial_{\mathbf{c}} \cdot \left[\dot{\theta} \mathbf{c} + \zeta_0 (1 + \gamma \theta c^2) (2\theta \mathbf{c} + \partial_{\mathbf{c}}) \right] \phi(\mathbf{c}, t) + K_d \sqrt{\theta} I[\mathbf{c}|\phi, \phi], \quad (19)$$

where θ is the temperature ratio—as defined in Eq. (12b), which equals unity at equilibrium, and

$$I[\mathbf{c}_1|\phi, \phi] = \int d\mathbf{c}_2 \int_+ d\hat{\sigma} \mathbf{c}_{12} \cdot \hat{\sigma} \times [\phi(\mathbf{c}'_1, t) \phi(\mathbf{c}'_2, t) - \phi(\mathbf{c}_1, t) \phi(\mathbf{c}_2, t)] \quad (20)$$

is the reduced collision operator with $\mathbf{c}_{12} \equiv \mathbf{c}_1 - \mathbf{c}_2$. For simplicity, in Eq. (19) and henceforth, the stars on t^* and ζ_0^* are dropped. In dimensionless variables, the evolution equation for the temperature, Eq. (13), reads

$$\frac{\dot{\theta}}{\zeta_0} = -2(\theta - 1) [1 + (d + 2)\gamma\theta] - 2(d + 2)\gamma\theta^2 a_2. \quad (21)$$

Multiplying both sides of Eq. (19) by c^ℓ and defining the reduced moments

$$M_\ell(t) \equiv \langle c^\ell \rangle = \int d\mathbf{c} c^\ell \phi(\mathbf{c}, t), \quad (22)$$

one obtains the hierarchy of equations [36]

$$\frac{\dot{M}_\ell}{\zeta_0} = \ell \left\{ \left[(\ell - 2)\gamma + (d + 2)\gamma\theta(1 + a_2) - \frac{1}{\theta} \right] M_\ell - 2\gamma\theta M_{\ell+2} + \frac{d + \ell - 2}{2} \frac{M_{\ell-2}}{\theta} \right\} - \frac{K_d}{\zeta_0} \sqrt{\theta} \mu_\ell, \quad (23)$$

where we have introduced the collisional moments μ_ℓ as

$$\mu_\ell \equiv - \int d\mathbf{c} c^\ell I[\mathbf{c}|\phi, \phi]. \quad (24)$$

Note that $M_0 = 1$, $M_2 = \frac{d}{2}$, and $M_4 = \frac{d(d+2)}{4}(1+a_2)$ [see Eq. (14)]. Conservation of mass and energy imply that $\mu_0 = \mu_2 = 0$, so that Eq. (23) is obviously consistent with $\dot{M}_0 = \dot{M}_2 = 0$.

Making use of the explicit form of the collision operator, it is possible to express the collisional moments as two-particle averages of the form

$$\mu_\ell = \int d\mathbf{c}_1 \int d\mathbf{c}_2 \phi(\mathbf{c}_1) \phi(\mathbf{c}_2) \Phi_\ell(\mathbf{c}_1, \mathbf{c}_2). \quad (25)$$

In particular, $\Phi_2 = 0$ and, after some algebra, one gets

$$\Phi_4(\mathbf{c}_1, \mathbf{c}_2) = \frac{2\pi^{\frac{d-1}{2}}}{\Gamma\left(\frac{d+5}{2}\right)} c_{12} [d(\mathbf{C} \cdot \mathbf{c}_{12})^2 - c_{12}^2 C^2], \quad (26a)$$

$$\Phi_6(\mathbf{c}_1, \mathbf{c}_2) = 3\Phi_4(\mathbf{c}_1, \mathbf{c}_2) \left(C^2 + \frac{c_{12}^2}{4} \right), \quad (26b)$$

where $\mathbf{C} \equiv \frac{1}{2}(\mathbf{c}_1 + \mathbf{c}_2)$ is the center-of-mass reduced velocity.

A. Sonine approximation

Let us first consider the case of linear drag, i.e., $\gamma = 0$. In that case, the LE state defined in Eq. (10) is an exact solution of the EFPE, Eq. (2). Equivalently, in reduced variables,

$$\phi^{\text{LE}}(\mathbf{c}) = \pi^{-d/2} e^{-c^2} \implies M_{2k}^{\text{LE}} = \frac{[d + 2(k-1)]!!}{2^k}, \quad (27)$$

becomes an exact stationary solution to Eqs. (19) and (23), because of the properties $I[\mathbf{c}|\phi^{\text{LE}}, \phi^{\text{LE}}] = 0$, $\mu_\ell^{\text{LE}} = 0$. Moreover, the solution to Eq. (21) is simply $\theta(t) = 1 + [\theta(0) - 1] e^{-2\zeta_0 t}$. Thus, if $\gamma = 0$ and the system is initially prepared in an equilibrium state with a temperature $T(0)$, its coupling to a bath at temperature T_b makes the temperature evolve toward T_b but otherwise the system remains always in local equilibrium, i.e., the VDF is Maxwellian with the time-dependent temperature.

Going back to the nonlinear case $\gamma \neq 0$, the VDF can be represented by the Sonine expansion

$$\phi(\mathbf{c}; t) = \phi^{\text{LE}}(\mathbf{c}) \left[1 + \sum_{j=2}^{\infty} a_j(t) L_j^{(\frac{d-2}{2})}(c^2) \right], \quad (28)$$

where $L_j^{(\frac{d-2}{2})}(c^2)$ are generalized Laguerre (or Sonine) polynomials and the coefficients $a_j = [j! \Gamma(\frac{d}{2}) / \Gamma(j + \frac{d}{2})] \langle L_j^{(\frac{d-2}{2})}(c^2) \rangle$ are the cumulants of the nonequilibrium VDF. The associated velocity moments are

$$M_{2k} = M_{2k}^{\text{LE}} \left[1 + \sum_{j=2}^k (-1)^j \binom{k}{j} a_j \right], \quad k \geq 2. \quad (29)$$

In particular,

$$M_6 = \frac{d(d+2)(d+4)}{8}(1+3a_2-a_3), \quad (30a)$$

$$M_8 = \frac{d(d+2)(d+4)(d+6)}{16}(1+6a_2-4a_3+a_4). \quad (30b)$$

The infinite moment hierarchy, Eq. (23), cannot be solved in an exact way in general. This is even the case for linear drag, $\gamma = 0$, when the initial state is not a Maxwellian. As a consequence, the exact evolution of the temperature ratio $\theta(t)$ cannot be obtained from Eq. (21).

Let us suppose, however, that the initial condition and subsequent evolution are sufficiently close to the LE state as to assume that the cumulants in Eq. (28) can be neglected beyond a_3 and the quadratic terms (i.e., those proportional to a_2^2 , a_3^2 , and a_2a_3) can be neglected as well. In that case, the two first nontrivial collisional moments become [74]

$$\mu_4 \approx \frac{2(d-1)}{K_d} \left(a_2 - \frac{a_3}{4} \right), \quad (31a)$$

$$\mu_6 \approx \frac{3(d-1)(2d+9)}{2K_d} \left(a_2 - \frac{3a_3}{4} \right). \quad (31b)$$

Within this scheme, Eq. (23) with $\ell = 4$ and $\ell = 6$ yields

$$\begin{aligned} \frac{\dot{a}_2}{\zeta_0} = & -8\gamma(\theta-1) + 4 \left[2\gamma - (d+8)\gamma\theta - \frac{1}{\theta} \right] a_2 \\ & + 4(d+4)\gamma\theta a_3 - \frac{8(d-1)}{d(d+2)} \frac{\sqrt{\theta}}{\zeta_0} \left(a_2 - \frac{a_3}{4} \right), \end{aligned} \quad (32a)$$

$$\begin{aligned} \frac{\dot{a}_3}{\zeta_0} = & -24\gamma(2-3\theta)a_2 + 6 \left[4\gamma - (d+14)\gamma\theta - \frac{1}{\theta} \right] a_3 \\ & + \frac{\sqrt{\theta}}{\zeta_0} \frac{3(d-1)}{d(d+2)(d+4)} [4a_2 - (4d+19)a_3]. \end{aligned} \quad (32b)$$

Equations (21) and (32) make a closed set of three coupled differential equations, nonlinear in the temperature but linear in the cumulants.

In this paper, we consider two Sonine approximations. The roughest approximation consists of neglecting a_3 , setting $a_3 = 0$ in Eq. (32a), and dealing then with Eqs. (21) and (32a) for the pair (θ, a_2) . Here, we term this approach the basic Sonine approximation (BSA) [75]. A more sophisticated theory is obtained by keeping a_3 and dealing then with Eqs. (21) and (32). We term this approach the extended Sonine approximation (ESA) [76].

III. THERMAL VERSUS ENTROPIC MPEMBA EFFECTS

A. Heuristic arguments

Now we proceed to study the ME in the theoretical framework of the Sonine approximations we have just

introduced. To start with, let us consider two samples (A and B) at the *same* initial temperatures $\theta_A(0) \equiv \theta_A^0$ and $\theta_B(0) \equiv \theta_B^0$, above the equilibrium value, i.e., $\theta_A^0 = \theta_B^0 > 1$. According to Eq. (21), the initial slopes $\dot{\theta}_A(0)$ and $\dot{\theta}_B(0)$ satisfy the inequality $\dot{\theta}_A(0) < \dot{\theta}_B(0)$ if $a_{2A}(0) \equiv a_{2A}^0 > a_{2B}(0) \equiv a_{2B}^0$, in which case sample A is expected to reach equilibrium before sample B. It must be brought to bear that the latter statement is true if $\theta(t) - 1$ keeps its initial sign along the whole relaxation to equilibrium, a condition that is assumed throughout this section. Exceptions to this fact are discussed in Sec. IV.

In order to analyze the TME described in Sec. I, let us take now $\theta_A^0 > \theta_B^0 > 1$. As discussed above, $\dot{\theta}_A(0) < \dot{\theta}_B(0)$ if $a_{2A}^0 > a_{2B}^0$. In that way, it can be expected that, by a convenient choice of the initial-condition values (θ_A^0, a_{2A}^0) and (θ_B^0, a_{2B}^0) , the evolution curves $\theta_A(t)$ and $\theta_B(t)$ intersect at a certain crossover time t_θ . That is, $\theta_A(t_\theta) = \theta_B(t_\theta)$ and $\dot{\theta}_A(t_\theta) < \dot{\theta}_B(t_\theta)$, which entails $a_{2A}(t_\theta) > a_{2B}(t_\theta)$ and $1 < \theta_A(t) < \theta_B(t)$ for $t > t_\theta$. This is the typical framework for the emergence of the (direct) TME in the kinetic description [36, 37, 39].

The inverse TME is analogous, except that, instead of $\theta_A^0 > \theta_B^0 > 1$, one now has $\theta_A^0 < \theta_B^0 < 1$. If now $a_{2B}^0 > a_{2A}^0$, then $\dot{\theta}_B(0) < \dot{\theta}_A(0)$, so that it is in principle possible that the evolution curve $\theta_A(t)$ intersects $\theta_B(t)$ at a certain crossover time t_θ . Note that here, without loss of generality, we denote by A the sample with an initial temperature farther from the equilibrium one, both in the direct and inverse TME.

In this work, we analyze both the TME and the EME. In the latter, it is the evolution curves of the relative entropy \mathcal{D} that intersect at a certain time $t_{\mathcal{D}}$, as described in Sec. I [77]. In particular, we want to understand whether the TME implies the EME or not. Also, when both the TME and the EME are present, we would like to investigate the relation between the crossing times t_θ and $t_{\mathcal{D}}$.

Let us address the questions above by simple heuristic arguments. First, we consider the case in which the further from equilibrium sample in the kinetic approach (A) is also the further from equilibrium in the entropic approach, i.e., $\mathcal{D}_A^0 > \mathcal{D}_B^0$. Therein, the existence of the TME implies that of the EME, and vice versa, as shown below. Note that $\mathcal{D}_A^0 > \mathcal{D}_B^0$ if \mathcal{D}^0 increases with $|\theta^0 - 1|$. This is indeed true for the LE contribution \mathcal{D}^{LE} , but not necessarily so for the total KLD \mathcal{D} if \mathcal{D}^{kin} plays a relevant role.

For the direct TME, we have $\theta_A^0 > \theta_B^0 > 1$ and $\mathcal{D}_A^0 > \mathcal{D}_B^0$. If the TME exists, then one has $\theta_B(t) > \theta_A(t) > 1$ after the crossover. In particular, this holds for sufficiently long times belonging to the hydrodynamic stage, where both $\mathcal{D}_A^{\text{kin}}$ and $\mathcal{D}_B^{\text{kin}}$ are negligible, and thus one has $\mathcal{D}_B(t) > \mathcal{D}_A(t)$ (EME) in the same stage. Reciprocally, if the EME exists, then $\mathcal{D}_B(t) > \mathcal{D}_A(t)$ in the hydrodynamic stage after the crossover, implying $\theta_B(t) > \theta_A(t) > 1$ (TME) in the same regime. An analogous reasoning applies to the inverse TME, i.e., $1 > \theta_B^0 > \theta_A^0$ and $\mathcal{D}_A^0 > \mathcal{D}_B^0$.

TABLE I. Summary of possible cases regarding the occurrence of the TME and the EME.

Case	Type of ME	Initial condition	If ...	then ...
ET1	Direct TME & EME	$\theta_A^0 > \theta_B^0 > 1$, $a_{2A}^0 > a_{2B}^0$, $\mathcal{D}_A^0 > \mathcal{D}_B^0$	$ a_{2A}(t_\theta) < a_{2B}(t_\theta) $	$t_D < t_\theta$
TE1	Direct TME & EME	$\theta_A^0 > \theta_B^0 > 1$, $a_{2A}^0 > a_{2B}^0$, $\mathcal{D}_A^0 > \mathcal{D}_B^0$	$ a_{2A}(t_\theta) > a_{2B}(t_\theta) $	$t_D > t_\theta$
ET2	Inverse TME & EME	$\theta_A^0 < \theta_B^0 < 1$, $a_{2A}^0 < a_{2B}^0$, $\mathcal{D}_A^0 > \mathcal{D}_B^0$	$ a_{2A}(t_\theta) < a_{2B}(t_\theta) $	$t_D < t_\theta$
TE2	Inverse TME & EME	$\theta_A^0 < \theta_B^0 < 1$, $a_{2A}^0 < a_{2B}^0$, $\mathcal{D}_A^0 > \mathcal{D}_B^0$	$ a_{2A}(t_\theta) > a_{2B}(t_\theta) $	$t_D > t_\theta$
T1	Direct TME	$\theta_A^0 > \theta_B^0 > 1$, $a_{2A}^0 > a_{2B}^0$	$\mathcal{D}_B^0 > \mathcal{D}_A^0$	No EME
T2	Inverse TME	$\theta_A^0 < \theta_B^0 < 1$, $a_{2A}^0 < a_{2B}^0$	$\mathcal{D}_B^0 > \mathcal{D}_A^0$	No EME
E1	EME	$\mathcal{D}_B^0 > \mathcal{D}_A^0$	$\theta_A^0 > \theta_B^0 > 1$	No Direct TME
E2	EME	$\mathcal{D}_B^0 > \mathcal{D}_A^0$	$\theta_A^0 < \theta_B^0 < 1$	No Inverse TME

Provided that the TME and EME are present, the argument above does not tell us the relative positioning of the crossover times t_θ and t_D , i.e., whether $t_\theta > t_D$ or $t_\theta < t_D$. Let us start by considering that the direct TME takes place at t_θ . Therefore, we have that $\mathcal{D}_A^{\text{LE}}(t_\theta) = \mathcal{D}_B^{\text{LE}}(t_\theta)$ and only the kinetic part contributes to the KLD difference at t_θ , $\mathcal{D}_A(t_\theta) - \mathcal{D}_B(t_\theta) = \mathcal{D}_A^{\text{kin}}(t_\theta) - \mathcal{D}_B^{\text{kin}}(t_\theta)$. This implies that $\mathcal{D}_A(t_\theta) < \mathcal{D}_B(t_\theta)$ (and hence $t_D < t_\theta$) if $\mathcal{D}_A^{\text{kin}}(t_\theta) < \mathcal{D}_B^{\text{kin}}(t_\theta)$, while $\mathcal{D}_A(t_\theta) > \mathcal{D}_B(t_\theta)$ (and hence $t_D > t_\theta$) otherwise.

For the sake of simplicity, and to go beyond the generic analysis of the previous paragraph, let us assume that the values of the excess kurtoses at the crossover time t_θ are small enough as to approximate $\mathcal{D}^{\text{kin}} \propto a_2^2$. The proportionality constant may depend on the details of the VDF—see below for the specific example of a gamma distribution. Within this approximation, the first case, $t_D < t_\theta$, is expected if $|a_{2A}(t_\theta)| < |a_{2B}(t_\theta)|$, while the second case, $t_D > t_\theta$, is expected if $|a_{2A}(t_\theta)| > |a_{2B}(t_\theta)|$. Both scenarios are possible, even recalling that $a_{2A}(t_\theta) > a_{2B}(t_\theta)$ is a necessary condition to have the TME, because the sign of the excess kurtoses of samples A and B may be different. For the case of the inverse TME, the sign of $t_D - t_\theta$ coincides again with that of $|a_{2A}(t_\theta)| - |a_{2B}(t_\theta)|$.

The different possibilities analyzed above for the case $\mathcal{D}_A^0 > \mathcal{D}_B^0$ are summarized in Table I, specifically as cases labeled ET1, TE1 (for the direct ME) and ET2, TE2 (for the inverse ME).

Now we move onto the situation in which the further from equilibrium sample in the kinetic approach (A) is, however, the closer to equilibrium in the entropic approach, $\mathcal{D}_A^0 < \mathcal{D}_B^0$. On account of Eq. (12b), the condition $\mathcal{D}_B^0 > \mathcal{D}_A^0$ requires

$$\mathcal{D}_B^{\text{kin},0} - \mathcal{D}_A^{\text{kin},0} > \frac{d}{2} \left(\theta_A^0 - \theta_B^0 - \ln \frac{\theta_A^0}{\theta_B^0} \right) > 0. \quad (33)$$

Additional cases are possible, which are labeled as T1, T2, E1, and E2 in Table I. The TME and the EME are no longer biunivocally related. For example, in the T1 case, the direct TME is present but no genuine EME takes place: $\theta_A^0 > \theta_B^0 > 1$ and $\theta_B(t) > \theta_A(t) > 1$ for $t > t_\theta$, but $\mathcal{D}_B > \mathcal{D}_A$ both initially and for asymptotically long times. Note, however, that this does not prevent the

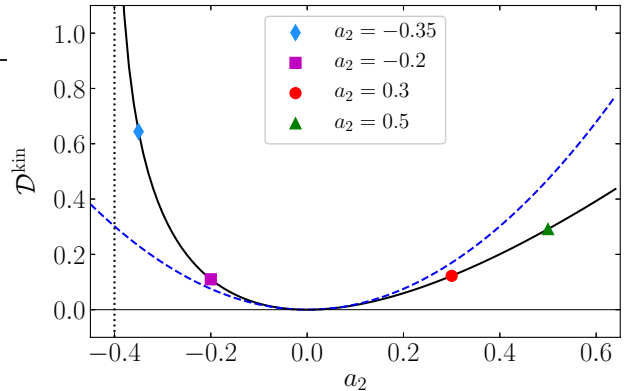


FIG. 1. Dependence of \mathcal{D}^{kin} with a_2 for a gamma distribution. Specifically, we plot the exact expression (solid line), given by Eq. (36), and the small $|a_2|$ approximation (dotted line), given by Eq. (37), for $d = 3$. Symbols correspond to the particular values at $a_2 = -0.35, -0.20, 0.30$, and 0.50 considered in Table II.

difference $\mathcal{D}_B(t) - \mathcal{D}_A(t)$ from changing its sign an even number of times during the transient relaxation.

To fix ideas and for further use, let us take the VDF corresponding to a gamma distribution [78] for the probability density of the variable $x = c^2$. Using the condition $\langle c^2 \rangle = \frac{d}{2}$, the reduced VDF associated with the gamma distribution reads

$$\phi(\mathbf{c}) = \pi^{-d/2} \frac{\Gamma(\frac{d}{2}) z^{dz/2}}{\Gamma(\frac{dz}{2})} c^{d(z-1)} e^{-zc^2}, \quad z \equiv \frac{1}{1 + \frac{d+2}{2} a_2}. \quad (34)$$

Note that this includes the LE distribution, Eq. (27), as the special case $a_2 = 0$. Thus, the deviations of the distribution (34) from LE are monitored by the excess kurtosis a_2 only. In particular, the sixth cumulant is given by

$$a_3 = \frac{4}{d+4} a_2 \left(1 - \frac{d+2}{2} a_2 \right). \quad (35)$$

The KLD of the gamma distribution with respect to

the LE one is [79]

$$\mathcal{D}^{\text{kin}} = \frac{d}{2} \left\{ \ln z + (z-1) \left[\psi \left(\frac{dz}{2} \right) - 1 \right] \right\} + \ln \frac{\Gamma \left(\frac{d}{2} \right)}{\Gamma \left(\frac{dz}{2} \right)}, \quad (36)$$

in which $\psi(x) = d \ln \Gamma(x)/dx$ is the digamma function [80]. For small $|a_2|$, one has

$$\mathcal{D}^{\text{kin}} \approx \frac{d(d+2)^2}{16} \left[\frac{d}{2} \psi' \left(\frac{d}{2} \right) - 1 \right] a_2^2, \quad (37)$$

where $\psi'(x) \equiv d\psi(x)/dx$.

The dependence of \mathcal{D}^{kin} , as given by Eq. (36), as a function of a_2 in the three-dimensional case ($d=3$) is shown in Fig. 1. We observe that \mathcal{D}^{kin} grows more rapidly for negative than for positive values of a_2 , exhibiting a vertical asymptote at $a_2 = -2/(d+2)$, which corresponds to $z \rightarrow \infty$.

B. Linearized analysis

To provide a simple, but yet more quantitative, study, let us adopt the linearization scheme put forward in Ref. [36]. The starting point is the BSA described by Eqs. (21) and (32a), setting $a_3 \rightarrow 0$ in the latter. Furthermore, the temperature ratio θ is linearized around a reference value θ_r close to $\theta^0 \equiv \theta(0)$. The solution of the resulting set of two differential equations is [36]

$$\begin{aligned} \theta(t) = & B_1 + [A_{11}(\theta^0 - B_1) - A_{12}(a_2^0 - B_2)] e^{-\lambda_- t} \\ & - [(A_{11} - 1)(\theta^0 - B_1) - A_{12}(a_2^0 - B_2)] e^{-\lambda_+ t}, \end{aligned} \quad (38a)$$

$$\begin{aligned} a_2(t) = & B_2 + [A_{22}(a_2^0 - B_2) - A_{21}(\theta^0 - B_1)] e^{-\lambda_- t} \\ & - [(A_{22} - 1)(a_2^0 - B_2) - A_{21}(\theta^0 - B_1)] e^{-\lambda_+ t}, \end{aligned} \quad (38b)$$

in which $a_2^0 \equiv a_2(0)$, and the expressions of the parameters λ_{\pm} , B_i , and A_{ij} can be found in Appendix B. We refer to Eqs. (38) as the linearized basic Sonine approximation (LBSA). When using the LBSA to investigate the ME, we are assuming that $\theta(t)$ is close to θ_r , which in turn is close to θ^0 : this entails that the LBSA is expected to be applicable to the kinetic stage only—i.e., when the ME comes about for short times.

The LBSA can be applied to the evolution of the two samples A and B with the convenient choice $\theta_r = \theta_B^0$ [36]. It is then straightforward to find the crossover time t_{θ} as

$$t_{\theta} = \frac{1}{\lambda_+ - \lambda_-} \ln \left(1 + \frac{A_{11}^{-1}}{R_{\text{max}}^0/R^0 - 1} \right), \quad (39)$$

where

$$R^0 \equiv \frac{\theta_A^0 - \theta_B^0}{a_{2A}^0 - a_{2B}^0}, \quad R_{\text{max}}^0 \equiv \frac{A_{12}}{A_{11}}. \quad (40)$$

TABLE II. Four representative choices for the initial values a_{2A}^0 and a_{2B}^0 ($d=3$). The numerical values of \mathcal{D}^{kin} , as given by Eq. (36) with $d=3$, are also included. The sixth column gives the cases (see Table I) that, in principle, are associated with each pair (a_{2A}^0, a_{2B}^0). However, some of them (enclosed in parentheses) are not actually observed (see Fig. 2).

Label	a_{2A}^0	a_{2B}^0	$\mathcal{D}_A^{\text{kin},0}$	$\mathcal{D}_B^{\text{kin},0}$	Cases
I	0.50	-0.35	0.292	0.644	ET1, (TE1), T1, E1, E2
II	0.50	-0.20	0.292	0.110	ET1, TE1
III	-0.35	0.30	0.644	0.122	ET2, TE2
IV	-0.20	0.50	0.110	0.292	(ET2), (TE2), T2, E1, E2

Therefore, in the LBSA, the crossover time t_{θ} depends on the set of four initial values θ_A^0 , a_{2A}^0 , θ_B^0 , and a_{2B}^0 only through the ratio R^0 . Moreover, Eq. (39) is meaningful only if

$$0 < R^0 < R_{\text{max}}^0. \quad (41)$$

Otherwise, no TME—either direct or inverse—exists.

The determination of the crossover time $t_{\mathcal{D}}$ is much more involved, even in the simple LBSA. It is obtained as the solution of a transcendental equation and the solution depends on θ_A^0 , a_{2A}^0 , θ_B^0 , and a_{2B}^0 . The locus separating the region where $t_{\mathcal{D}} < t_{\theta}$ from the region where $t_{\mathcal{D}} > t_{\theta}$ is approximately given by the condition $|a_{2A}(t_{\theta})| = |a_{2B}(t_{\theta})|$; the sign of $t_{\mathcal{D}} - t_{\theta}$ is the same as that of $|a_{2A}(t_{\theta})| - |a_{2B}(t_{\theta})|$ —as discussed in the previous section. See cases ET1, TE1, ET2, and TE2 in Table I. Furthermore, cases T1, T2, E1, and E2 are possible if the initial values of the KLD cross the locus $\mathcal{D}_A^0 = \mathcal{D}_B^0$, as summarized in Table I and described in Sec. III A. If the locus $\mathcal{D}_A^0 = \mathcal{D}_B^0$ happens to separate regions ET1 and T1 (or ET2 and T2), then one has $t_{\mathcal{D}} \rightarrow 0$ on the locus, so that $0 < t_{\mathcal{D}} < t_{\theta}$ in region ET1 (or ET2) and formally $t_{\mathcal{D}} < 0 < t_{\theta}$ in region T1 (or T2).

C. Illustrative examples

Let us choose the four representative pairs (a_{2A}^0, a_{2B}^0) presented in Table II. Since the scenarios ET1 and TE1 described in Table I require $a_{2A}^0 > a_{2B}^0$, they are *in principle* feasible for the pairs I and II. Analogously, the scenarios ET2 and TE2 might be possible for the pairs III and IV. Next, by assuming the initial VDF has the gamma form, Eq. (34), we have $\mathcal{D}_B^{\text{kin},0} > \mathcal{D}_A^{\text{kin},0}$ for the pairs I and IV, but not for the pairs II and III; in view of Eq. (33), we conclude that, *in principle*, cases T1, E1, and E2 are possible for pair I and cases T2, E1, and E2 for pair IV.

The phase diagrams predicted by the LBSA are shown in Fig. 2 for $\zeta_0 = 1$, $\gamma = 0.1$, and $d = 3$. We observe that, at least for that choice of the parameters, case TE1 is absent for the class of initial conditions I, while cases ET2 and TE2 are absent for the class of initial conditions IV.

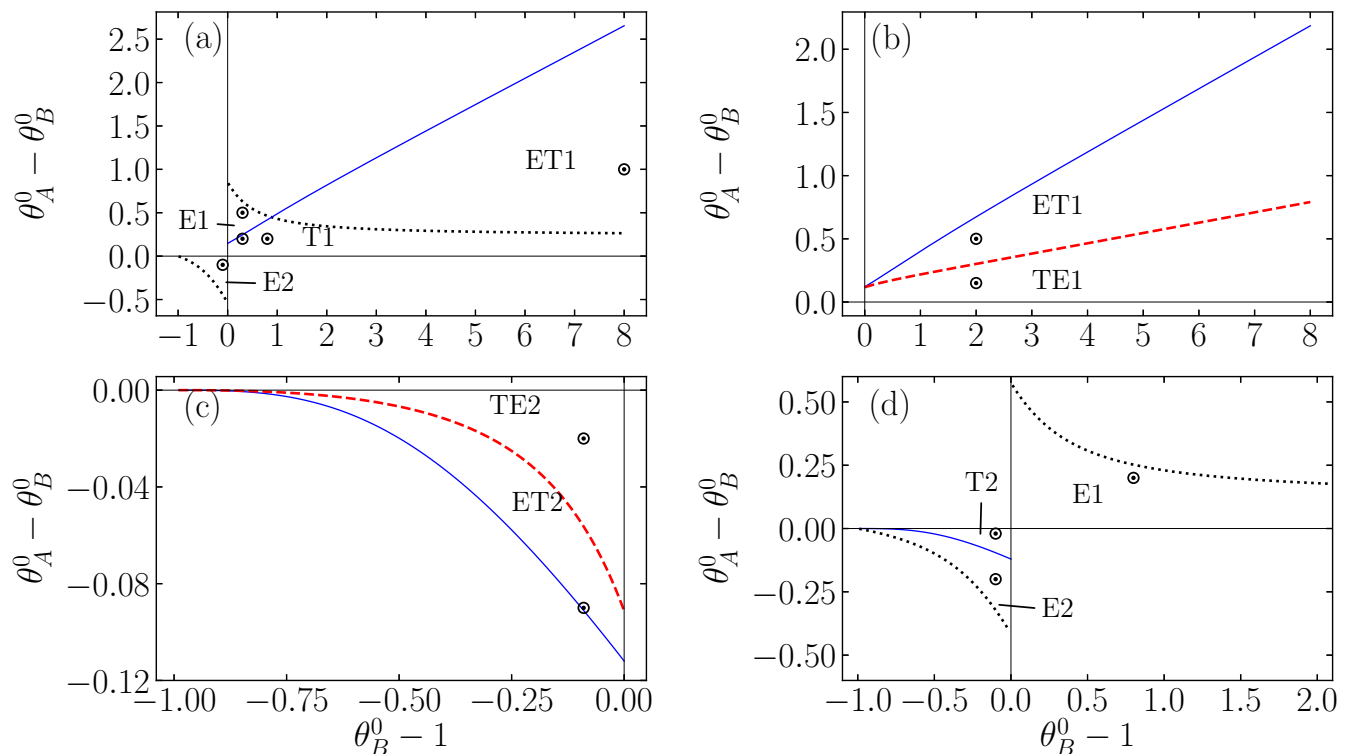


FIG. 2. Phase diagrams in the representation $\theta_A^0 - \theta_B^0$ vs $\theta_B^0 - 1$. Specifically, they are plotted for $\zeta_0 = 1$, $\gamma = 0.1$, $d = 3$, and the four representative choices of (a_{2A}^0, a_{2B}^0) displayed in Table II: (a) I, (b) II, (c) III, and (d) IV. The solid, dashed, and dotted lines represent the loci $R^0 = R_{\max}^0$, $t_\theta = t_D$, and $\mathcal{D}_A^0 = \mathcal{D}_B^0$, respectively. The labels in each region correspond to the cases described in Table I and the circles represent the specific examples considered in Figs. 3–6. Note that $\theta_A^0 > \theta_B^0 > 1$ and $\theta_A^0 < \theta_B^0 < 1$ refer to the direct TME and inverse TME, respectively.

The time evolution of the differences

$$\Delta\mathcal{D} \equiv \mathcal{D}_A - \mathcal{D}_B, \quad \Delta\mathcal{D}^{\text{LE}} \equiv \mathcal{D}_A^{\text{LE}} - \mathcal{D}_B^{\text{LE}} \quad (42)$$

for the representative points indicated in Fig. 2 are displayed in Figs. 3–6. The change of sign of $\mathcal{D}_A^{\text{LE}} - \mathcal{D}_B^{\text{LE}}$ and $\mathcal{D}_A - \mathcal{D}_B$ during their evolution signals the presence of the TME and EME, respectively. Here, we made an extra ansatz to evaluate $\mathcal{D}^{\text{kin}}(t)$. As we are working with an initial gamma distribution and the final equilibrium state is a particular case of such a distribution—with $a_2 = 0$, we have assumed that the VDF during its time evolution is sufficiently close to a gamma distribution so as to estimate $\mathcal{D}^{\text{kin}}(t)$ by Eq. (36) with an excess kurtosis $a_2(t)$ given by Eq. (38b).

Figures 3(b) and 3(c) are both examples of the scenario T1 for the class of initial conditions I. In Fig. 3(b), where $(\theta_B^0 - 1, \theta_A^0 - \theta_B^0) = (0.8, 0.2)$ [see Fig. 2(a)], the difference $\mathcal{D}_A^0 - \mathcal{D}_B^0$ presents a negative local maximum. When moving horizontally in Fig. 2(a) to the point $(\theta_B^0 - 1, \theta_A^0 - \theta_B^0) = (0.3, 0.2)$, however, Fig. 3(c) shows that the local maximum of $\mathcal{D}_A^0 - \mathcal{D}_B^0$ becomes positive and $\mathcal{D}_A^0 - \mathcal{D}_B^0$ vanishes twice during the time evolution. While interesting, this does not qualify as an EME because, as already said above Eq. (33), $\mathcal{D}_B > \mathcal{D}_A$ both initially and for asymptotically long times. Next, moving vertically

in Fig. 2(a) to the point $(\theta_B^0 - 1, \theta_A^0 - \theta_B^0) = (0.3, 0.5)$, the local maximum observed in Fig. 3(d) is again positive but there is a single crossing $\mathcal{D}_A^0 - \mathcal{D}_B^0 = 0$, which results in the E1 scenario.

IV. KOVACS-INDUCED MPEMBA EFFECT

In Sec. III, we have assumed that, even though the evolution of $\theta(t)$ may not be monotonic, $\theta(t) - 1$ does not change sign, i.e., there is no crossover with the equilibrium value. However, such a crossover $\theta(t_K) = 1$ at a finite time t_K is possible. In general, $a_2(t_K) \neq 0$, and Eq. (21) shows that $\dot{\theta}(t_K)/\zeta_0\gamma = -2(d+2)a_2(t_K) \neq 0$. As a consequence, starting from $\theta^0 > 1$, $\theta(t) - 1$ develops a hump with a negative minimum if $a_2(t_K) > 0$; analogously, starting from $\theta^0 < 1$, $\theta(t) - 1$ develops a hump with a positive maximum if $a_2(t_K) < 0$. Because of its formal analogy with the Kovacs effect [37, 81–87], we will refer to this crossover $\theta(t_K) = 1$ and subsequent hump, either positive or negative, as a Kovacs-like phenomenon.

Given the fact that the relaxation of $a_2(t)$ is generally much faster than that of $\theta(t)$, at least if $\theta^0 = O(1)$ [37], it is reasonable to expect that the Kovacs-like effect requires initial values $|\theta^0 - 1| \ll 1$, unless $|a_2^0|$ is unphysically large.

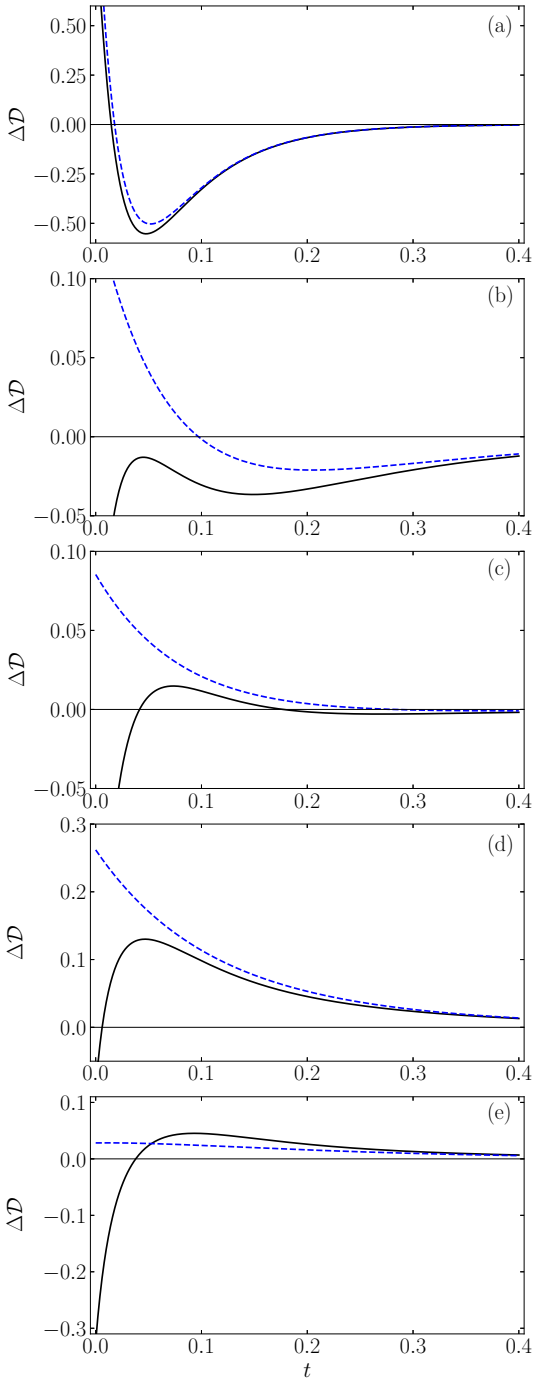


FIG. 3. Time evolution of the relative entropy for the representative initial condition I for (a_{2A}^0, a_{2B}^0) in Table II. Parameter values are $\zeta_0 = 1$, $\gamma = 0.1$, $d = 3$. Specifically, we represent $\mathcal{D}_A^{\text{LE}} - \mathcal{D}_B^{\text{LE}}$ (dashed lines) and $\mathcal{D}_A - \mathcal{D}_B$ (solid lines) for different pairs of initial temperatures, namely: (a) $(\theta_A^0, \theta_B^0) = (10, 9)$, (b) $(\theta_A^0, \theta_B^0) = (2, 1.8)$, (c) $(\theta_A^0, \theta_B^0) = (1.5, 1.3)$, (d) $(\theta_A^0, \theta_B^0) = (1.8, 1.3)$, (e) $(\theta_A^0, \theta_B^0) = (0.8, 0.91)$. Panels (a), (b), (c), (d) and (e) represent examples of cases ET1, T1, T1, E1, and E2, respectively.

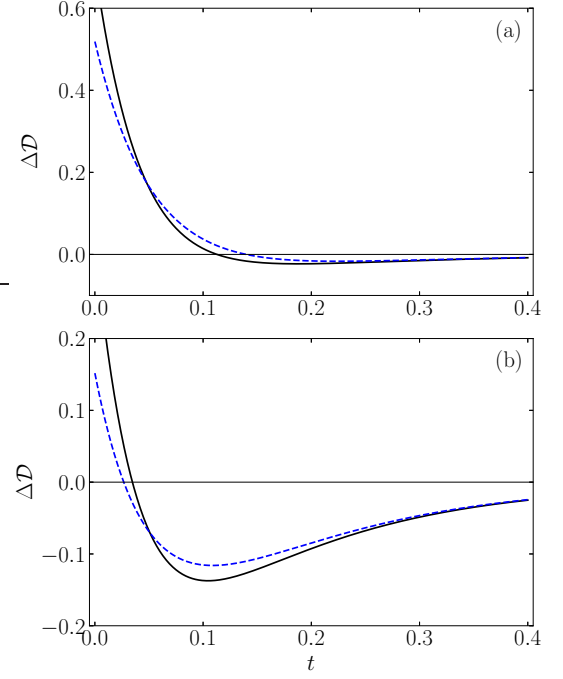


FIG. 4. Same as in Fig. 3, but now for the representative initial condition II for (a_{2A}^0, a_{2B}^0) . Here, initial conditions for the temperatures are: (a) $(\theta_A^0, \theta_B^0) = (3.5, 3)$, (b) $(\theta_A^0, \theta_B^0) = (3.15, 3)$. Panels (a) and (b) represent examples of cases ET1 and TE1, respectively.

This suggests a theoretical treatment based on the LBSA (38) with $\theta_r \rightarrow 1$, i.e.,

$$\theta(t) = 1 + [\bar{A}_{11}(\theta^0 - 1) - \bar{A}_{12}a_2^0] e^{-\bar{\lambda}_- t} - [(\bar{A}_{11} - 1)(\theta^0 - 1) - \bar{A}_{12}a_2^0] e^{-\bar{\lambda}_+ t}, \quad (43a)$$

$$a_2(t) = [\bar{A}_{22}a_2^0 - \bar{A}_{21}(\theta^0 - 1)] e^{-\bar{\lambda}_- t} - [(\bar{A}_{22} - 1)a_2^0 - \bar{A}_{21}(\theta^0 - 1)] e^{-\bar{\lambda}_+ t}, \quad (43b)$$

where overlined quantities refer to their values at $\theta_r = 1$. Following the same methodology as in Eqs. (39) and (40), we find

$$t_K = \frac{1}{\bar{\lambda}_+ - \bar{\lambda}_-} \ln \left[1 + \frac{\bar{A}_{11}^{-1}}{\bar{R}_{\max}^0 a_2^0 / (\theta^0 - 1) - 1} \right], \quad (44)$$

where

$$\bar{R}_{\max}^0 \equiv \frac{\bar{A}_{12}}{\bar{A}_{11}}. \quad (45)$$

Therefore, according to the LBSA, the Kovacs-like effect appears if

$$0 < \frac{\theta^0 - 1}{a_2^0} < \bar{R}_{\max}^0. \quad (46)$$

It is interesting to look into the possible change of the ME phenomenology brought about by the Kovacs-like

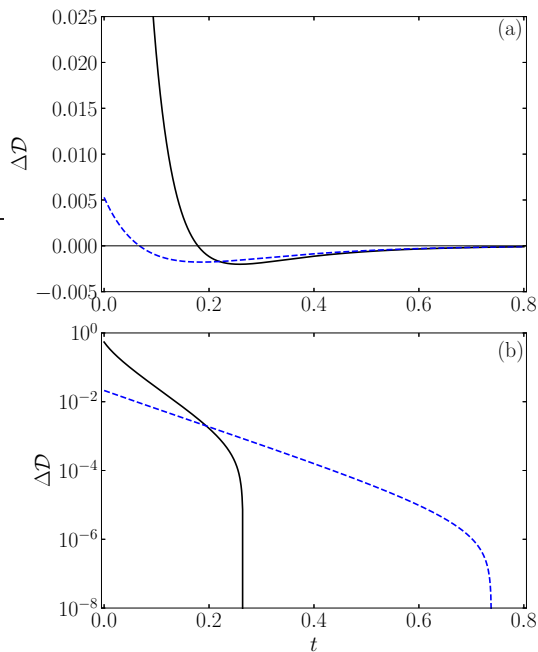


FIG. 5. Same as in Fig. 3, but now for the representative initial condition III for (a_{2A}^0, a_{2B}^0) . In this case, the initial conditions for the temperatures chosen are: (a) $(\theta_A^0, \theta_B^0) = (0.88, 0.91)$, (b) $(\theta_A^0, \theta_B^0) = (0.82, 0.91)$. Panels (a) and (b) represent examples of cases TE2 and ET2, respectively. Note that $\Delta\mathcal{D}$ is plotted in logarithmic times in panel (b) to favor the perception of the crossover times, at which $\Delta\mathcal{D}$ vanishes.

humps. As we show below, the existence of humps may make it necessary to change the preconception of considering the TME present only when the evolution curves of the temperature of the two samples intersect. To be more specific, we consider, as before, samples A and B with A being the initially hotter, i.e., $\theta_A^0 > \theta_B^0 > 1$. Let us assume that the colder sample B fulfills condition (46) but the hotter sample does not. In that case, $\theta_B(t)$ might not be crossed by the curve $\theta_A(t)$, which remains always above the equilibrium temperature, and yet relax more slowly to equilibrium than A but from below. We could then say that a (direct) TME is present without the existence of a standard crossover time t_θ , provided that a crossover between the LE KLD curves $\mathcal{D}_A^{\text{LE}}(t)$ and $\mathcal{D}_B^{\text{LE}}(t)$ occurs at a certain time $t_{\mathcal{D}^{\text{LE}}}$. A completely analogous situation is possible for the inverse ME, i.e., when $\theta_A^0 < \theta_B^0 < 1$. We will refer to this phenomenon, where $\mathcal{D}_A^{\text{LE}}$ and $\mathcal{D}_B^{\text{LE}}$ intersect but $\theta_A(t)$ and $\theta_B(t)$ do not, as the Kovacs-induced ME (KIME). This phenomenon is reminiscent of the ME observed in Ref. [21] in supercooled water.

The different scenarios where Kovacs-like humps appear are illustrated in Fig. 7 for direct preparations, i.e., $\theta_A^0 > \theta_B^0 > 1$. In Fig. 7(a), $\theta_A(t)$ and $\theta_B(t)$ do not cross each other, but they both exhibit Kovacs-like humps, the one in system B being stronger than in system A. This

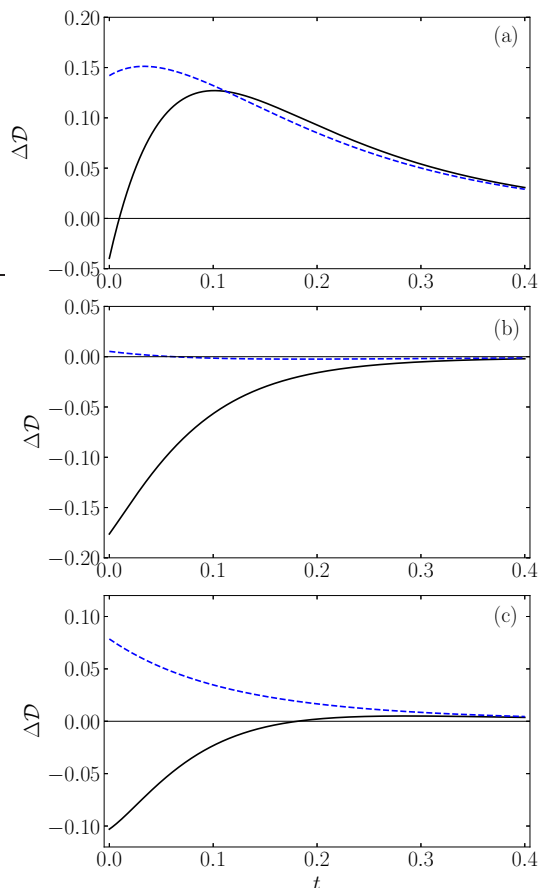


FIG. 6. Same as in Fig. 3, but now for the representative initial condition IV for (a_{2A}^0, a_{2B}^0) . Here, initial temperatures are: (a) $(\theta_A^0, \theta_B^0) = (2, 1.8)$, (b) $(\theta_A^0, \theta_B^0) = (0.88, 0.91)$, (c) $(\theta_A^0, \theta_B^0) = (0.7, 0.91)$. Panels (a), (b), and (c) represent examples of cases E1, T2, and E2, respectively.

makes the latter system relax to equilibrium earlier than the former, what physically qualifies as a direct TME. Whereas in the thermal scheme there is no crossing, the positiveness of \mathcal{D}^{LE} forces an intersection between A and B curves, as observed in Fig. 7(b). This is the essence of the KIME.

On the other hand, the existence of humps or of a finite crossover time t_θ does not ensure the existence of TME. In fact, in Fig. 7(c) there is a crossing between the thermal curves, but the Kovacs-like humps make the initially hotter system relax later to the equilibrium state, thus frustrating the TME. This is signaled by a pair of intersections in the \mathcal{D}^{LE} curves of Fig. 7(d), so the KIME is absent. The third different scenario is reflected in Figs. 7(e) and 7(e)(f), where there is no crossover either in the thermal evolution or in \mathcal{D}^{LE} , even though sample B exhibits a thermal hump.

The analogous cases for inverse preparations $\theta_A^0 < \theta_B^0 < 1$ are illustrated in Fig. 8.

To sum up, the KIME is characterized by a single crossing $\mathcal{D}_A^{\text{LE}} = \mathcal{D}_B^{\text{LE}}$ at a certain time $t_{\mathcal{D}^{\text{LE}}}$, without any cross-

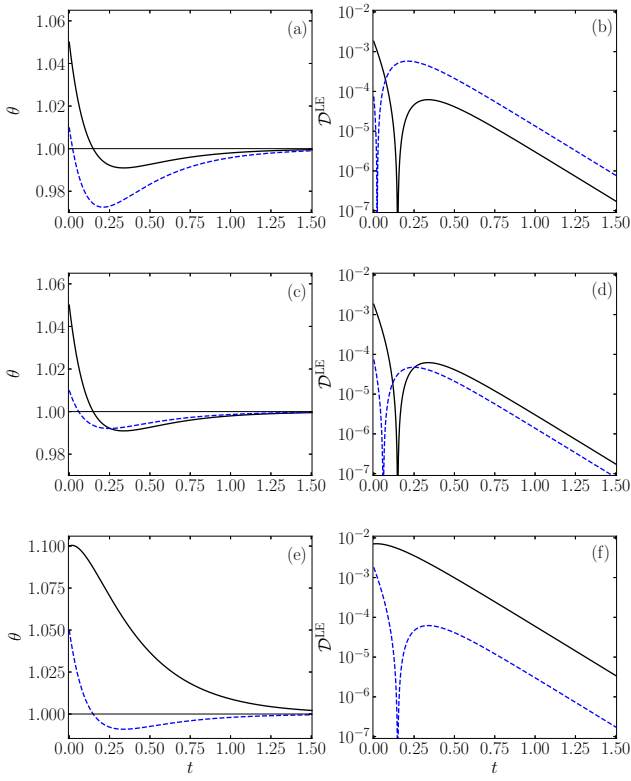


FIG. 7. Time evolution of the temperature and LE relative entropy of samples A and B for the direct case, $\theta_A^0 > \theta_B^0 > 1$. Specifically, we show $\{\theta_A, \mathcal{D}_A^{\text{LE}}\}$ (solid lines) and $\{\theta_B, \mathcal{D}_B^{\text{LE}}\}$ (dashed lines), as obtained from Eq. (43a). Initial conditions are: (a, b) $(\theta_A^0, \theta_B^0) = (1.05, 1.01)$ and $(a_{2A}^0, a_{2B}^0) = (0.5, 0.5)$, (c, d) $(\theta_A^0, \theta_B^0) = (1.05, 1.01)$ and $(a_{2A}^0, a_{2B}^0) = (0.5, 0.2)$, and (e, f) $(\theta_A^0, \theta_B^0) = (1.1, 1.05)$ and $(a_{2A}^0, a_{2B}^0) = (-0.35, 0.5)$. In all cases, $\zeta_0 = 1$, $\gamma = 0.1$, and $d = 3$.

ing between θ_A and θ_B . In order to establish the conditions under which this may happen, let us assume again $|\theta - 1| \ll 1$ and approximate $\ln \theta \approx \theta - 1 - \frac{1}{2}(\theta - 1)^2$ in Eq. (12b). Therefore, the condition $\mathcal{D}_A^{\text{LE}}(t_{\mathcal{D}^{\text{LE}}}) = \mathcal{D}_B^{\text{LE}}(t_{\mathcal{D}^{\text{LE}}})$ with $\theta_A(t_{\mathcal{D}^{\text{LE}}}) \neq \theta_B(t_{\mathcal{D}^{\text{LE}}})$ translates into

$$\theta_A(t_{\mathcal{D}^{\text{LE}}}) - 1 = 1 - \theta_B(t_{\mathcal{D}^{\text{LE}}}). \quad (47)$$

Making use of Eq. (43a) entails

$$t_{\mathcal{D}^{\text{LE}}} = \frac{1}{\lambda_+ - \lambda_-} \ln \left(1 + \frac{\bar{A}_{11}^{-1}}{\bar{R}_{\text{max}}^0 / R_+^0 - 1} \right), \quad (48)$$

where \bar{R}_{max}^0 is defined in Eq. (45) and

$$R_+^0 \equiv \frac{\theta_A^0 + \theta_B^0 - 2}{a_{2A}^0 + a_{2B}^0}. \quad (49)$$

Note the difference between this parameter R_+^0 and the parameter R^0 defined before in Eq. (40). Since $t_{\mathcal{D}^{\text{LE}}}$ must be finite in the KIME, the corresponding condition on the initial preparation is

$$0 < R_+^0 < \bar{R}_{\text{max}}^0, \quad (50a)$$

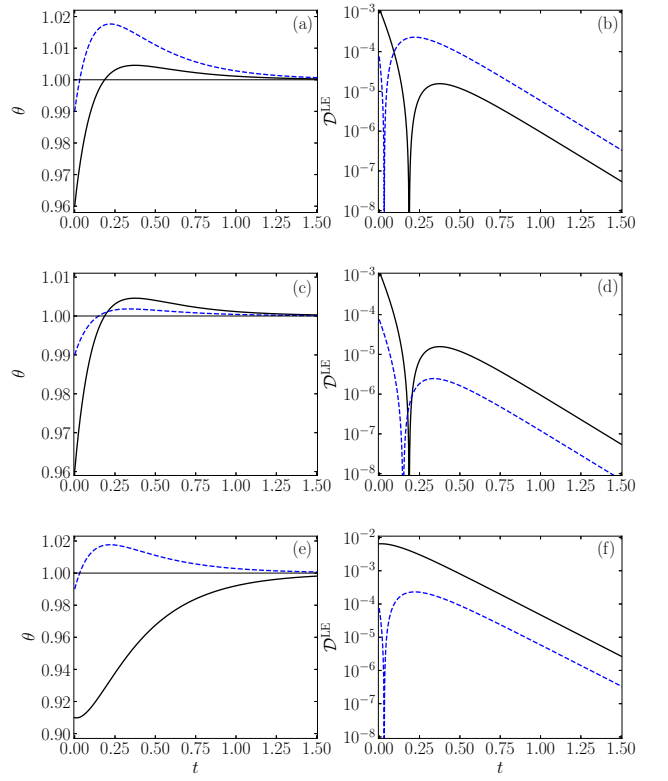


FIG. 8. Same as in Fig. 7, but now for the inverse case $\theta_A^0 < \theta_B^0 < 1$. Initial conditions are: (a, b) $(\theta_A^0, \theta_B^0) = (0.96, 0.99)$ and $(a_{2A}^0, a_{2B}^0) = (-0.35, -0.35)$, (c, d) $(\theta_A^0, \theta_B^0) = (0.96, 0.99)$ and $(a_{2A}^0, a_{2B}^0) = (-0.35, -0.1)$, and (e, f) $(\theta_A^0, \theta_B^0) = (0.91, 0.99)$ and $(a_{2A}^0, a_{2B}^0) = (0.3, -0.35)$.

$$R^0 < 0 \text{ or } R^0 > \bar{R}_{\text{max}}^0. \quad (50b)$$

The supplementary condition (50b) represents the violation of Eq. (41) (with $\theta_r \rightarrow 1$) and is needed to exclude any thermal crossing.

According to Eq. (46), if both systems A and B exhibit Kovacs-like humps, the condition given by Eq. (50a) is ensured. As a test, note that $R_{\text{max}}^0 = 0.172$ for all the cases considered in Figs. 7 and 8. The values of (R_+^0, R^0) are $(0.060, \infty)$, $(0.086, 0.133)$, and $(1, -0.059)$ in the cases represented in panels (a, b), (c, d), and (e, f) of Fig. 7. Analogously, (R_+^0, R^0) are $(0.071, \infty)$, $(0.111, 0.120)$, and $(2, -0.123)$ in the cases represented in panels (a, b), (c, d), and (e, f) of Fig. 8, respectively. Thus, the KIME double condition (50) is fulfilled only in the cases (a, b) of Figs. 7 and 8.

V. SIMULATION RESULTS

In this section, our simulation results are used to test the theoretical predictions stemming from the numerical solutions of: (i) the (nonlinear) BSA, Eqs. (21) and (32a) with $a_3 \rightarrow 0$, and ESA, Eqs. (21) and (32). The theoretical results for the KLD $\mathcal{D}(t)$ and $\mathcal{D}^{\text{LE}}(t)$ are con-

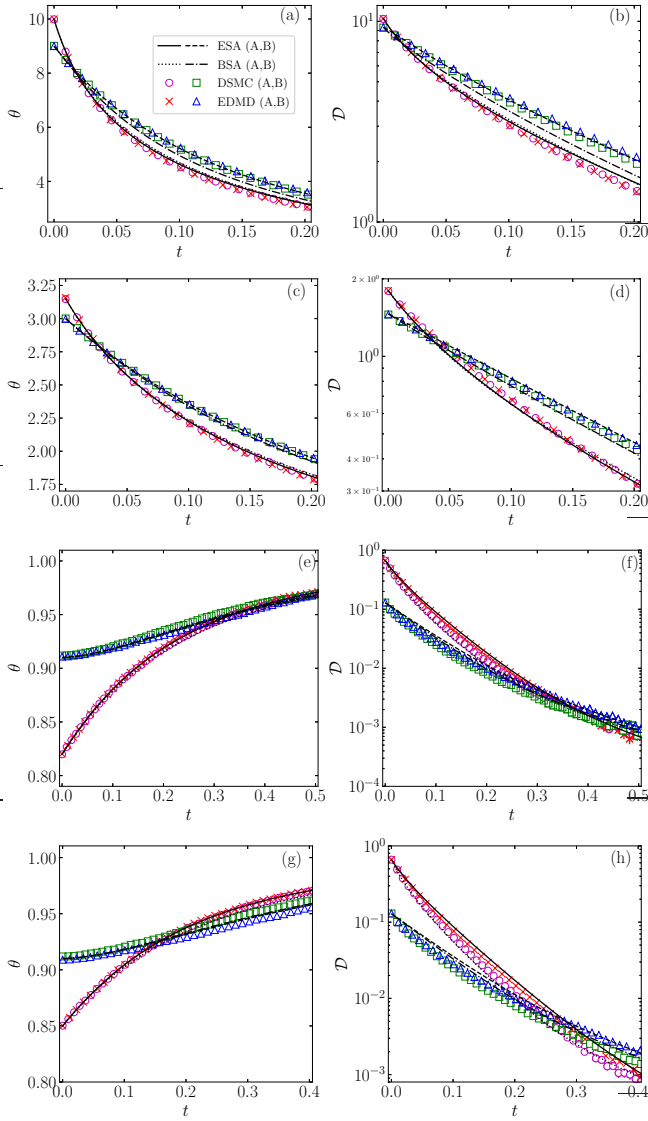


FIG. 9. ME for cases when $\theta - 1$ does not change its sign. Specifically, we plot the time evolution of the temperature and relative entropy for samples A and B: $\{\theta_A, \mathcal{D}_A\}$ (solid and dotted lines, circles, and crosses) and $\{\theta_B, \mathcal{D}_B\}$ (dashed and dash-dotted lines, squares, and triangles). Initial conditions are: (a, b) $(\theta_A^0, \theta_B^0) = (10, 9)$ and $(a_{2A}^0, a_{2B}^0) = (0.5, -0.35)$, (c, d) $(\theta_A^0, \theta_B^0) = (3.15, 3)$ and $(a_{2A}^0, a_{2B}^0) = (0.5, -0.2)$, (e, f) $(\theta_A^0, \theta_B^0) = (0.82, 0.91)$ and $(a_{2A}^0, a_{2B}^0) = (-0.35, 0.3)$, and (g, h) $(\theta_A^0, \theta_B^0) = (0.85, 0.91)$ and $(a_{2A}^0, a_{2B}^0) = (-0.35, 0.3)$. Other parameter values are $\zeta_0 = 1$, $\gamma = 0.1$, and $d = 3$.

structured by introducing the theoretical $\theta(t)$ and $a_2(t)$ in Eqs. (12b) and (36), respectively.

The employed computer simulation schemes, DSMC and EDMD, to build the simulation curves are presented in Appendix C. In all cases, the (reduced) initial VDF has been taken as the gamma distribution given by Eq. (34) with the chosen value of the initial excess kurtosis a_2^0 , as previously done in Refs. [39, 88, 89]. The KLD from simulations is computed as described in Refs. [88, 89].

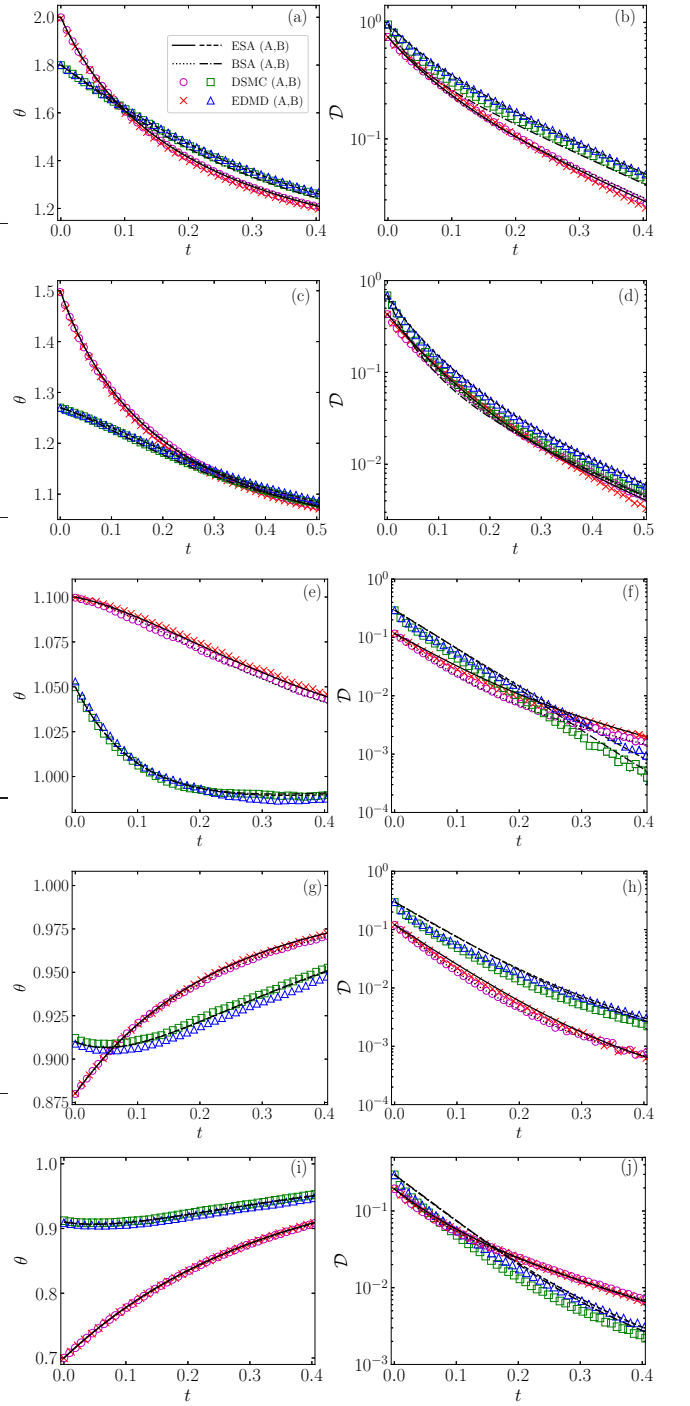


FIG. 10. Same as in Fig. 9, except that the initial conditions are: (a-d) $(\theta_A^0, \theta_B^0) = (2, 1.8)$ and $(a_{2A}^0, a_{2B}^0) = (0.5, -0.35)$, (e-h) $(\theta_A^0, \theta_B^0) = (1.5, 1.27)$ and $(a_{2A}^0, a_{2B}^0) = (0.5, -0.35)$, (i-l) $(\theta_A^0, \theta_B^0) = (1.1, 1.05)$ and $(a_{2A}^0, a_{2B}^0) = (-0.35, 0.5)$, (m-p) $(\theta_A^0, \theta_B^0) = (0.88, 0.91)$ and $(a_{2A}^0, a_{2B}^0) = (-0.2, 0.5)$, and (q-t) $(\theta_A^0, \theta_B^0) = (0.7, 0.91)$ and $(a_{2A}^0, a_{2B}^0) = (-0.2, 0.5)$.

Figures 9 and 10 contain the theoretical and simulation results of the time evolution of the temperature ratio θ and the KLD \mathcal{D} . The graphs for the cumulants a_2 and

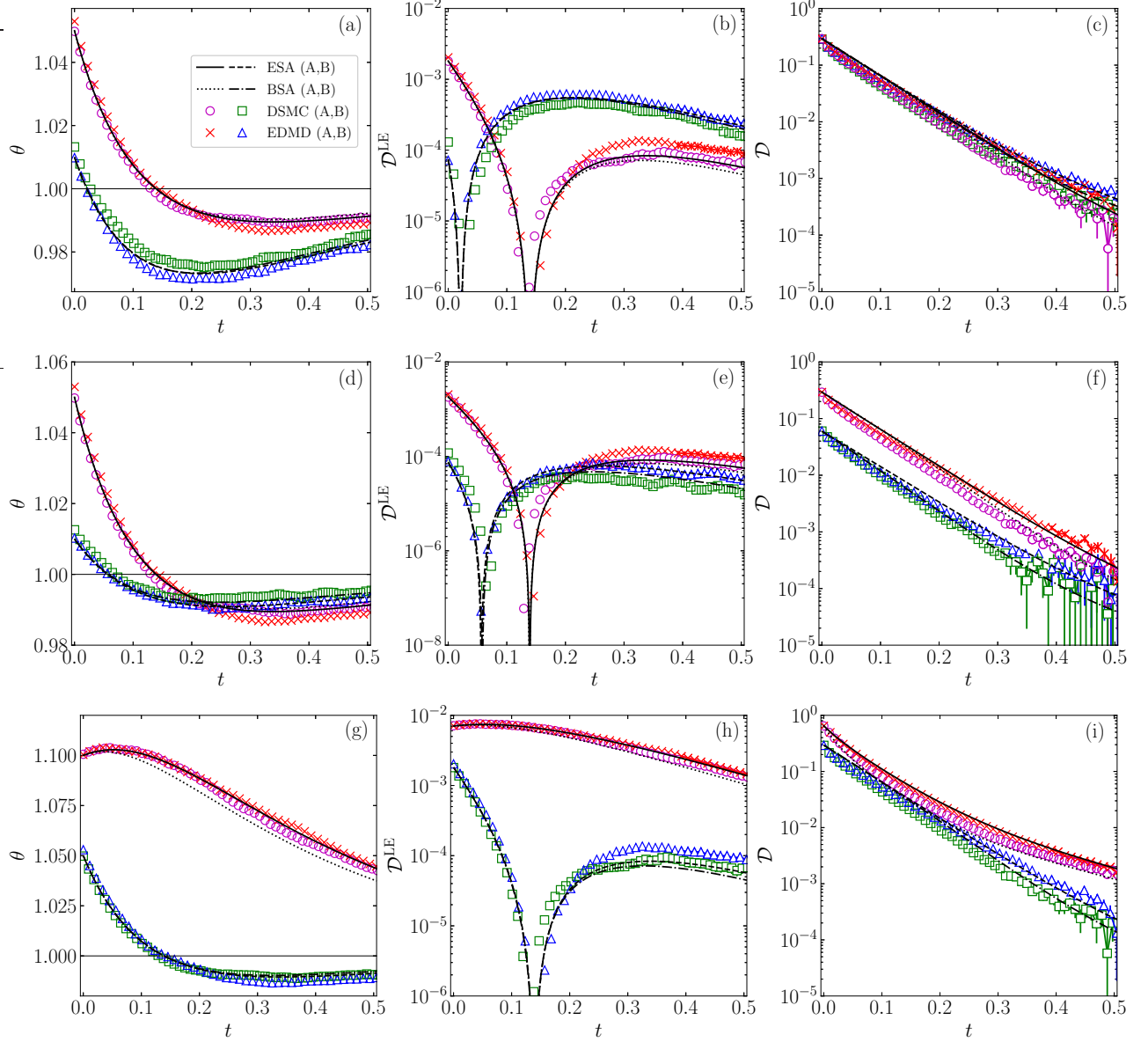


FIG. 11. ME for cases case in which $\theta - 1$ changes sign, i.e., the KIME. In this case, we show the time evolution of: $\{\theta_A, \mathcal{D}_A^{\text{LE}}, \mathcal{D}_A\}$ (solid and dotted lines, circles, and crosses) and $\{\theta_B, \mathcal{D}_B^{\text{LE}}, \mathcal{D}_B\}$ (dashed and dash-dotted lines, squares, and triangles). Parameter values and initial conditions correspond to those in Fig. 7.

a_3 are presented in Appendix D. Samples A and B are prepared with the representative values of the cumulants in Table II, namely pairs I and II (III and IV) for the direct (inverse) ME, and different values of the initial temperatures θ_A^0 and θ_B^0 . Pairs (θ_A^0, θ_B^0) are chosen to illustrate the different cases summarized in Table I. Specifically, we present the cases ET1 in Figs. 9(a, b), TE1 in Figs. 9(c, d), ET2 in Figs. 9(e, f), TE2 in Figs. 9(g, h), T1 in Figs. 10(a, b), T1 with a double crossing in \mathcal{D} in Figs. 10(c, d), E1 in Figs. 10(e, f), T2 in Figs. 10(g, h), and E2 in Figs. 10(i, j). Note that the cases in Figs. 9(a, b), 9(c, d), 9(e, f), 10(a, b), 10(g, h), and 10(i, j) are the same as in Figs. 3(a), 4(b), 5(b), 3(b), 6(b), and 6(c),

respectively. Moreover, the case in Figs. 10(c, d) is close to the case in Fig. 3(c).

It must be remarked that the classification of the case in Figs. 9(e, f) as ET2 is less clear than expected. The LBSA theory predicts the ET2 behavior with a wide difference between t_θ and $t_{\mathcal{D}}$, as observed in panel (b) of Fig. 5(b). Still, nonlinearities reduce the time difference $t_\theta - t_{\mathcal{D}}$. Moreover, the double crossing in \mathcal{D} predicted by the LBSA for the case of Figs. 10(c, d) is not actually observed in the simulations. The shallow positive maximum of $\mathcal{D}_A - \mathcal{D}_B$ predicted by the LBSA, as seen in panel (c) of Fig. 3(c), is washed out by nonlinear contributions—at least in the case represented in Figs. 10(c, d).

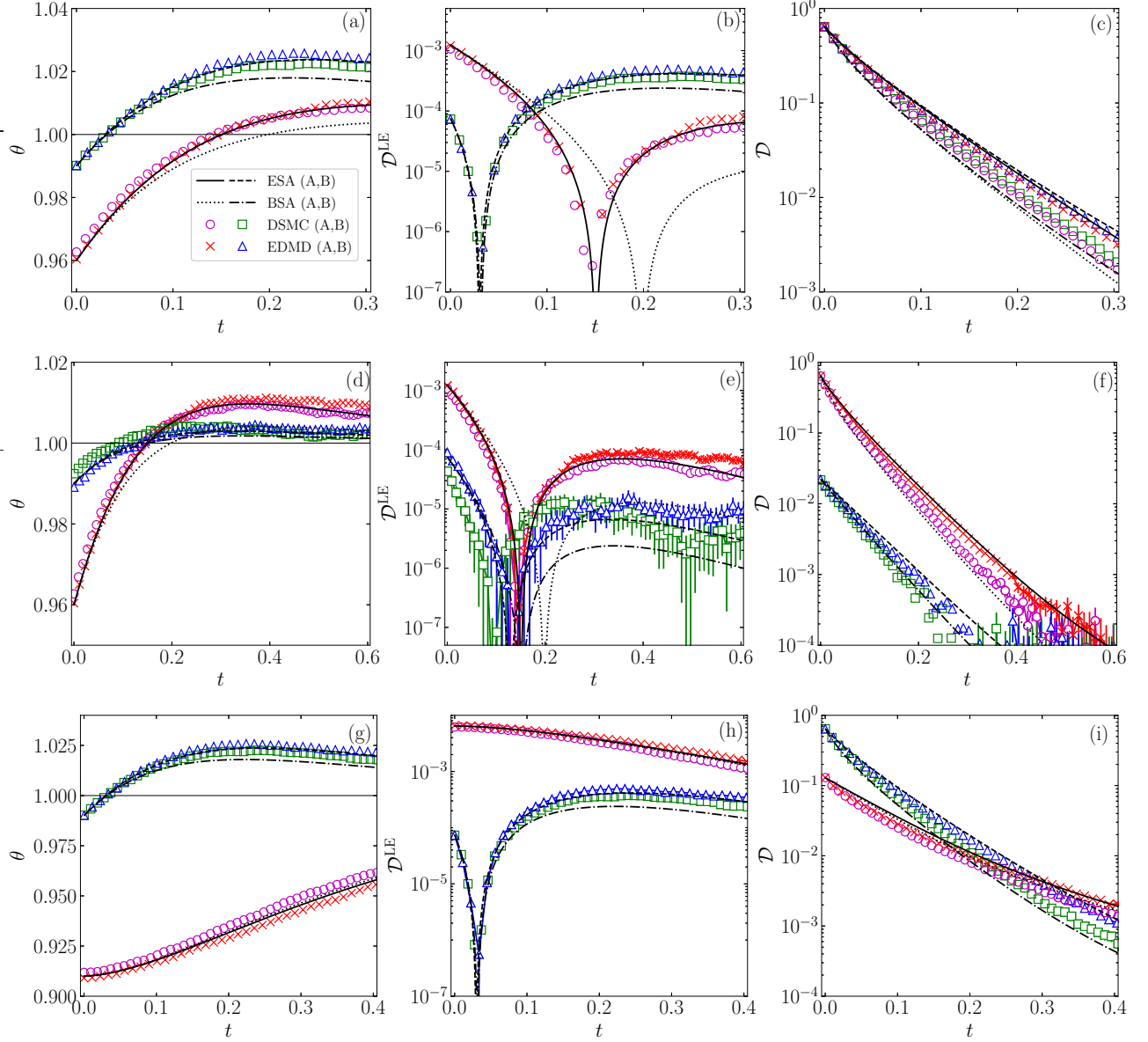


FIG. 12. Same as in Fig. 11, but now for the initial conditions in Fig. 8.

Let us now turn to the KIME predicted by the LBSA, which we have discussed in Sec. IV. Figures 11 and 12 show the time evolution of θ , \mathcal{D}^{LE} , and \mathcal{D} for the same cases as considered in Figs. 7 and 8, respectively. Again, the graphs for a_2 and a_3 can be found in Appendix D. We see that the Kovacs-like behavior and the KIME phenomenology are indeed present. The crossover characterizing the TME is accounted for by the intersection of the \mathcal{D}^{LE} curves in Figs. 11(a-c) and 12(a-c), though the corresponding temperature curves never cross.

The figures in this section show that our theoretical predictions for both $\theta(t)$ and $\mathcal{D}(t)$ are generally in very good agreement with DSMC and EDMD simulation results. This is especially true for the ESA, which still gives a good account of the behavior of the fourth cumulant

$a_2(t)$ and a fair account of the behavior of the sixth cumulant $a_3(t)$ (see Figs. 15–18), consistently with the results reported in Ref. [37]. The improvement of the ESA over the BSA can be understood by noticing that the values of the cumulant a_3 are typically of the same magnitude as those of a_2 . It is also worth highlighting the generally good agreement between the simulation results for the relative entropy \mathcal{D} and those obtained from Eqs. (12b) and (36) when θ and a_2 are given by either the BSA or the ESA. This means that the gamma distribution in Eq. (34) represents a convenient proxy of the unknown time-dependent VDF. This ansatz is further confirmed by the generally fair agreement (not shown) between the simulation data for a_3 and the right-hand-side of Eq. (35) when plugging the simulation data of a_2 , especially in the

cases with $a_2 < 0$.

Finally, we note that small deviations between EDMD and DSMC simulation are observed (especially for the subtler quantities \mathcal{D} and a_3), despite the low density of the systems. This might be a consequence of the approximations carried out in the numerical implementation of the Langevin dynamics in the AGF algorithm explained in Appendix C 2. Nevertheless, there is a good agreement for the collisional scheme, as tested in Appendix C 3.

VI. CONCLUSIONS

In this paper, we have analyzed in depth the relaxation to equilibrium of a dilute gas of elastic hard spheres subjected to a nonlinear drag and the associated stochastic force. We have particularly focused on two versions of the ME, namely, the TME and the EME. Our analysis combines theory and simulation. The theoretical approach is based on a Sonine expansion of the solution of the EFPE, Eq. (2). The simulation approach comprises both DSMC results, which integrate numerically Eq. (2), and EDMD results.

We have employed the Kullback–Leibler divergence (or relative entropy) \mathcal{D} , defined in Eq. (9), to measure the distance to equilibrium and monitor the possible emergence of the EME. It must be remarked that other distances to equilibrium have been employed in the literature, as long as they share some common properties of monotonicity, convexity, etc. However, the choice of the distance function does not impinge on the existence of the EME—for a thorough discussion of this issue, see Ref. [50]. The KLD choice for the distance function is especially convenient for our comparing the TME and EME, since \mathcal{D} can be decomposed into two summands, see Eqs. (11) and (12). First, the hydrodynamic LE contribution \mathcal{D}^{LE} , which only depends on the temperature and, second, the kinetic-stage correction \mathcal{D}^{kin} , which depends on the whole VDF. To obtain an approximate expression for the latter within the Sonine approximation, we have employed the gamma distribution function, Eq. (36).

For given values of the drag force, i.e., given values of (ζ_0, γ) , the emergence of ME—either direct or inverse—depends on the initial preparations of the two samples A, whose initial temperature is farther from equilibrium, and B, whose initial temperature is closer to equilibrium. The simplest approach, based on heuristic arguments, is the LBSA given by Eqs. (38). Therein, both the temperature ratio $\theta(t)$ and the excess kurtosis $a_2(t)$ are a linear superposition of two exponentials.

When the difference $\theta - 1$ keeps its initial sign during the relaxation process—i.e., when the temperature does not cross its equilibrium value at a finite time, we have the most usual, standard situation. Bringing to bear that the kinetic-stage contribution \mathcal{D}^{kin} is expected to decay to zero over a shorter time scale than that of the local equilibrium contribution \mathcal{D}^{LE} , we have argued that the

existence of TME implies that of EME (and vice versa) if $\mathcal{D}_A^0 > \mathcal{D}_B^0$. There are two possibilities: either the thermal crossover occurs earlier than the entropic one (scenarios TE1 and TE2 for direct and inverse effects, respectively) or it occurs later than the entropic crossover (scenarios ET1 and ET2 for direct and inverse effects, respectively).

Interestingly, even though θ_A^0 departs from the equilibrium value 1 more than θ_B^0 , one may have $\mathcal{D}_A^0 < \mathcal{D}_B^0$ due to the contribution \mathcal{D}^{kin} to the entropic distance. This gives rise to the existence of TME without entropy crossover (scenarios T1 and T2 for direct and inverse effects, respectively) or, reciprocally, the existence of EME without thermal crossover (scenarios E1 and E2 for direct and inverse effects, respectively).

A summary of all the possible scenarios above—for constant sign of $\theta - 1$ —is provided by Table I. The corresponding phase diagrams in the plane $\theta_A^0 - \theta_B^0$ vs $\theta_B^0 - 1$ are depicted in Fig. 2 for a few representative choices of the initial excess kurtoses a_{2A}^0 and a_{2B}^0 , given in Table II. Those scenarios are modified when the condition of constant sign of $\theta(t) - 1$ is violated, as explained below.

Nonmonotonic evolutions of θ with a crossing of the equilibrium line $\theta = 1$ induce the appearance of Kovacs-like humps. Sample B may relax to equilibrium later than sample A when the temperature of the former overshoots the equilibrium value, a fact that sample A can take advantage of. Even though $\theta_A(t)$ and $\theta_B(t)$ do not intersect, the corresponding curves of \mathcal{D}^{LE} do intersect. Because of the signature of a Kovacs-like hump, we have termed this class of ME as KIME. Simple conditions for its existence, Eqs. (50), have been derived by adapting the LBSA to this situation.

We argue that the KIME implies a revision of the conventional definition of TME. Provided that both initial temperatures are either above (direct case) or below (inverse case) equilibrium, the TME is not necessarily characterized by the crossover of the nonequilibrium temperature but by the crossover of the associated positive-definite quantity \mathcal{D}^{LE} . Within this generalized scheme and for a general complex system, we propose that the TME exists in a pair of different initially prepared setups if there are an odd number of crossings between their LE relative entropy \mathcal{D}^{LE} curves. Analogously, the EME exists if there are an odd number of crossings during the corresponding time evolution of the whole relative entropy \mathcal{D} .

The different scenarios above, emerging in the extremely simplistic LBSA, have been tested and confirmed by computer simulations (both DSMC and EDMD). These numerical results have also been compared with the more complex nonlinear BSA and ESA. The inclusion of the additional cumulant a_3 in the set of coupled evolution equations allows the ESA to improve over the BSA. Moreover, DSMC and EDMD results are practically indistinguishable, with small discrepancies that can be traced back to the approximations in the EDMD scheme during the free streaming stage, see Appendix C 2. On the other hand, the collisional schemes are tested

in Appendix C3, with good results.

We expect this work can motivate the experimental investigation, making use of a suitable aging protocol to prepare the initial samples, of the whole variety of ME phenomenology described in this work. Specifically, our predicting and observing the KIME—as a novel unexpected behavior—in this molecular gas driven by a nonlinear drag, opens the door to its finding in other complex systems. Also, we plan to employ the theoretical and computational framework developed here to study the relaxation times of pairs of temperature quenches thermodynamically equidistant from equilibrium [90, 91], one above and the other one below.

ACKNOWLEDGMENTS

A.M. and A.S. acknowledge financial support from Grant PID2020-112936GB-I00 funded by MCIN/AEI/10.13039/501100011033, and from grants IB20079 and GR21014 funded by Junta de Extremadura (Spain) and by ERDF “A way of making Europe.” A.P. acknowledges financial support from Grant PGC2018-093998-B-I00 funded by MCIN/AEI/10.13039/501100011033/ and by ERDF “A way of making Europe.” A.M. is grateful to the Spanish Ministerio de Ciencia, Innovación y Universidades for a predoctoral fellowship FPU2018-3503.

Appendix A: Langevin Equation under Nonlinear Drag

In this Appendix we discuss the Langevin equation associated with the left-hand side of Eq. (2), since the effect of interparticle collisions represented by the right-hand side is well known.

Let us start writing the Langevin equation as

$$\dot{\mathbf{v}}(t) = -\zeta(v(t))\mathbf{v}_i(t) + \xi(v(t))\boldsymbol{\eta}(t), \quad (\text{A1})$$

where $\boldsymbol{\eta}(t)$ is a Gaussian white-noise stochastic term with the statistical properties

$$\langle \boldsymbol{\eta}(t) \rangle_{\text{noise}} = 0, \quad \langle \boldsymbol{\eta}(t)\boldsymbol{\eta}(t') \rangle_{\text{noise}} = \mathbf{l}\delta(t-t'), \quad (\text{A2})$$

where \mathbf{l} is the $d \times d$ unit tensor and $\langle \cdot \rangle_{\text{noise}}$ reads for an average over different realizations. Let us define a Wiener process $W(t)$ with elemental increment $dW(t) = \xi(v(t))\boldsymbol{\eta}(t)dt$. This is the case of a multiplicative noise and, therefore, there is no a unique way of interpreting the proper time within a given interval $[t, t+h]$ at which the process $W(t)$ must be evaluated [92]. In general, one can choose a time $t + \epsilon h$ parameterized by $0 \leq \epsilon \leq 1$. Hence, the associated Fokker–Planck equation is [92]

$$\partial_t f(\mathbf{v}) - \frac{\partial}{\partial \mathbf{v}} \cdot \left[\zeta(v)\mathbf{v} + \frac{\xi^{2\epsilon}(v)}{2} \frac{\partial}{\partial \mathbf{v}} \xi^{2(1-\epsilon)}(v) \right] f(\mathbf{v}) = 0. \quad (\text{A3})$$

The specific choices $\epsilon = 0, \frac{1}{2}$, and 1 correspond to the Itô [64], Stratonovich [64], and Klimontovich [93] interpretations, respectively.

The (differential) fluctuation-dissipation relation stemming from Eq. (A3) turns out to be

$$\zeta(v) = \frac{m\xi^2(v)}{2k_B T_b} - \frac{1-\epsilon}{2v} \frac{\partial \xi^2(v)}{\partial v}. \quad (\text{A4})$$

Only in the Klimontovich interpretation ($\epsilon = 1$) does one recover the conventional fluctuation-dissipation relation, Eq. (4), holding for constant drag coefficient and additive noise. In that case, the left-hand sides of Eqs. (2) and (A3) coincide.

On the other hand, from a simulation point of view, the Itô interpretation ($\epsilon = 0$) is the simplest one to implement. Fortunately, even if $\epsilon \neq 0$ (as happens in the Stratonovich and Klimontovich interpretations), one can always apply the Itô interpretation to the Langevin equation, provided that the original drag coefficient $\zeta(v)$ is replaced by an effective one ζ_{eff} (“spurious drift”). Note first the mathematical identity

$$\xi^{2\epsilon}(v) \frac{\partial}{\partial \mathbf{v}} \xi^{2(1-\epsilon)}(v) f(\mathbf{v}) = \frac{\partial}{\partial \mathbf{v}} \xi^2(v) f(\mathbf{v}) - \epsilon \frac{\partial \xi^2(v)}{\partial v} f(\mathbf{v}). \quad (\text{A5})$$

Inserting this into Eq. (A3), one gets

$$\partial_t f(\mathbf{v}) - \frac{\partial}{\partial \mathbf{v}} \cdot \left[\zeta_{\text{eff}}(v)\mathbf{v} + \frac{\partial \xi^2(v)}{\partial v} \frac{1}{2} \right] f(\mathbf{v}) = 0, \quad (\text{A6})$$

where

$$\begin{aligned} \zeta_{\text{eff}}(v) &\equiv \zeta(v) - \frac{\epsilon}{2v} \frac{\partial \xi^2(v)}{\partial v} \\ &= \frac{m\xi^2(v)}{2k_B T_b} - \frac{1}{2v} \frac{\partial \xi^2(v)}{\partial v}. \end{aligned} \quad (\text{A7})$$

In the particular case of Eq. (6) and $\epsilon = 1$, the effective drag coefficient becomes

$$\zeta_{\text{eff}}(v) = \zeta(v) - 2\zeta_0\gamma. \quad (\text{A8})$$

Thus, the original Langevin equation, Eq. (A1), in the Klimontovich interpretation is equivalent to the Langevin equation

$$\dot{\mathbf{v}}(t) = -\zeta_{\text{eff}}(v(t))\mathbf{v}(t) + \xi(v(t))\boldsymbol{\eta}(t) \quad (\text{A9})$$

in the Itô interpretation.

Appendix B: Parameters in Eqs. (38)

The parameters λ_{\pm} , B_i , and A_{ij} are given by

$$\lambda_{\pm} = \frac{\Lambda_{11} + \Lambda_{22} \pm \sqrt{(\Lambda_{11} - \Lambda_{22})^2 + 4\Lambda_{12}\Lambda_{21}}}{2}, \quad (\text{B1a})$$

$$B_1 = \theta_r + \frac{\Lambda_{22}C_1 - \Lambda_{12}C_2}{\Lambda_{11}\Lambda_{22} - \Lambda_{12}\Lambda_{21}}, \quad B_2 = \frac{\Lambda_{11}C_2 - \Lambda_{21}C_1}{\Lambda_{11}\Lambda_{22} - \Lambda_{12}\Lambda_{21}}, \quad (\text{B1b})$$

$$A_{11} = \frac{\lambda_+ - \Lambda_{11}}{\lambda_+ - \lambda_-}, \quad A_{22} = \frac{\lambda_+ - \Lambda_{22}}{\lambda_+ - \lambda_-}, \quad (\text{B1c})$$

$$A_{12} = \frac{\Lambda_{12}}{\lambda_+ - \lambda_-}, \quad A_{21} = \frac{\Lambda_{21}}{\lambda_+ - \lambda_-}, \quad (\text{B1d})$$

where

$$\Lambda_{11} = 2\zeta_0 [1 + (d+2)\gamma(2\theta_r - 1)], \quad (\text{B2a})$$

$$\Lambda_{22} = \zeta_0 \left[\frac{4}{\theta_r} - 8\gamma + 4(d+8)\gamma\theta_r \right] + \frac{8(d-1)}{d(d+2)}\sqrt{\theta_r}, \quad (\text{B2b})$$

$$\Lambda_{12} = 2\zeta_0(d+2)\gamma\theta_r^2, \quad \Lambda_{21} = 8\zeta_0\gamma, \quad (\text{B2c})$$

$$C_1 = 2\zeta_0(1 - \theta_r)[1 + (d+2)\gamma\theta_r], \quad C_2 = 8\zeta_0\gamma(1 - \theta_r). \quad (\text{B2d})$$

Appendix C: Computer Simulation Schemes

We have performed DSMC and EDMD simulations of the model to test the theoretical predictions. In both schemes, the nonlinear drag is implemented at the level of stochastic equations of motion by using Eq. (A9) and applying the associated Wiener process at time t within the interval $[t, t+h]$.

1. Direct Simulation Monte Carlo

The implementation of DSMC for this system is based in the pioneering work by Bird [94, 95], except for our taking into account of both the nonlinear drag and white-noise forces during the free-streaming stage of the algorithm [96].

Let us assume a homogeneous system of N particles, where their dynamics is just controlled by their velocities $\{\mathbf{v}_i\}$ with $i = 1, \dots, N$, and positions are obviated. The discrete VDF of such a system of particles is given by

$$n^{-1}f(\mathbf{v}, t) = \frac{1}{N} \sum_{i=1}^N \delta(\mathbf{v}_i(t) - \mathbf{v}). \quad (\text{C1})$$

At the initialization of the system, the squared moduli of the particles velocities $\{v_i^2(0)\}$ are drawn from a gamma distribution parameterized by $\langle v^2(0) \rangle = dk_B T^0/m$ and $\langle v^4(0) \rangle = d(d+2)(k_B T^0/m)^2(1 + a_2^0)$. Next, the velocity vectors $\{\mathbf{v}_i(0)\}$ are constructed from these moduli, with random directions. To enforce a vanishing initial total momentum, the velocity of every particle is subsequently subtracted by the amount $N^{-1} \sum_i \mathbf{v}_i(0)$.

After initialization, velocities are updated from t to $t+h$ (where the time step h is much smaller than the mean free time) by splitting the algorithm into two different stages: collisions and free streaming.

During the collision stage, a number $\frac{1}{2}N\omega_{\max}h$ of pairs are randomly chosen with uniform probability, where ω_{\max} is an upper bound estimate for the collision rate of one particle. Then, given a pair ij , the collision is accepted (acceptance-rejection Metropolis criterion) with probability $\Theta(\mathbf{v}_{ij} \cdot \hat{\boldsymbol{\sigma}}_{ij})\omega_{ij}/\omega_{\max}$, where $\hat{\boldsymbol{\sigma}}_{ij}$ a random vector in the unit d -sphere and $\omega_{ij} = \Omega_d \sigma^{d-1} n g_c |\mathbf{v}_{ij} \cdot \hat{\boldsymbol{\sigma}}_{ij}|$ with $\Omega_d = 2\pi^{d/2}/\Gamma(d/2)$ being the d -dimensional solid angle. If the collision is accepted for the given pair, postcollisional velocities are assigned following the collisional rules for elastic hard spheres, namely $\mathbf{v}_{i,j} \rightarrow \mathbf{v}_{i,j} \mp (\mathbf{v}_{ij} \cdot \hat{\boldsymbol{\sigma}}_{ij})\hat{\boldsymbol{\sigma}}_{ij}$. If $\omega_{ij} > \omega_{\max}$ in one of the sampled pairs, the collision is accepted and the estimate is updated as $\omega_{\max} = \omega_{ij}$.

During free streaming, velocities are updated according to the scheme given by (A9), namely

$$\mathbf{v}_i(t) \rightarrow \mathbf{v}_i(t+h) \approx \mathbf{v}_i(t) - \zeta_{\text{eff}}(v_i(t))\mathbf{v}_i(t)h + \xi(v_i(t))\sqrt{h}\mathbf{Y}_i + \mathcal{O}(h^{3/2}), \quad (\text{C2})$$

where \mathbf{Y}_i is a random vector drawn from the Gaussian probability distribution

$$P(\mathbf{Y}) = (2\pi)^{-d/2} e^{-Y^2/2}. \quad (\text{C3})$$

In our DSMC algorithm we took $N = 10^4$ three-dimensional particles ($d = 3$) and chose a time step $h = 10^{-2}\lambda/\sqrt{2k_B T_b/m}$, where $\lambda = (\sqrt{2}\pi n\sigma^2)^{-1}$ is the mean free path.

2. Event Driven Molecular Dynamics

EDMD algorithms are based in the evolution driven by events which can be particle-particle collisions, boundary effects, or other more complex interactions. Between two consecutive events, there is a free streaming of particles. Again, the stochastic and drag forces directly influence the particle dynamics. Whereas in DSMC positions were not required, in EDMD they are essential and are affected by the nonlinear noise, as explained below.

In order to implement the effect of the Langevin dynamics in our EDMD simulations, we have followed the *Approximate Green function* (AGF) algorithm proposed in Ref. [97]. Since $\dot{\mathbf{r}}_i(t) = \mathbf{v}(t)$, Eq. (C2) must be supplemented by [97]

$$\mathbf{r}_i(t) \rightarrow \mathbf{r}_i(t+h) \approx \mathbf{r}_i(t) + \mathbf{v}_i(t)h \left[1 - \frac{\zeta_{\text{eff}}(v_i(t))}{2}h \right] + \frac{1}{2}\xi(v_i(t))h^{3/2}\mathbf{W}_i + \mathcal{O}(h^{5/2}), \quad (\text{C4})$$

with

$$\mathbf{W}_i = \mathbf{Y}_i + \sqrt{\frac{5}{3}}\bar{\mathbf{Y}}_i, \quad (\text{C5})$$

where we have particularized the algorithm to the three-dimensional geometry, \mathbf{Y}_i is the random vector appearing

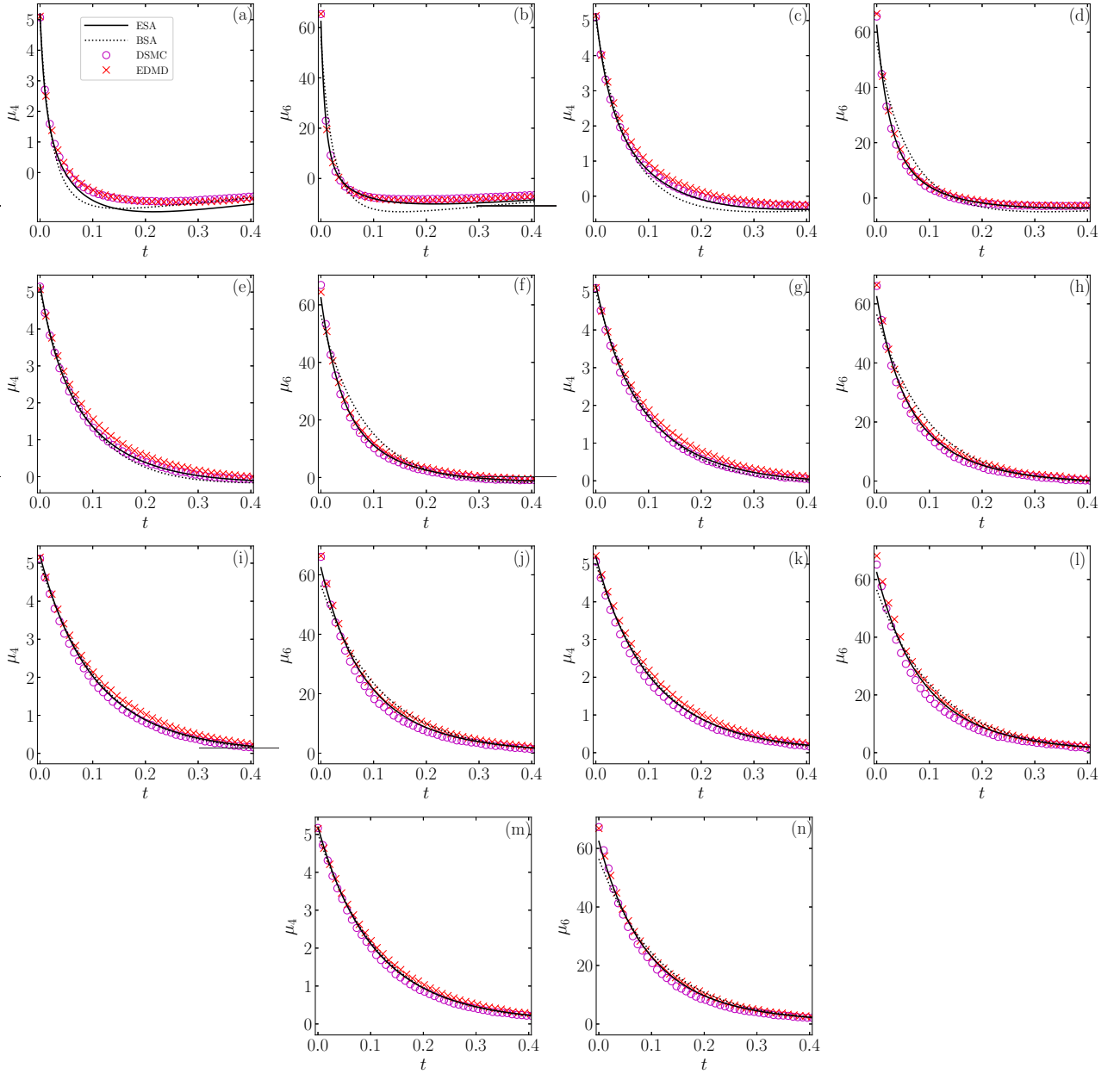


FIG. 13. Evolution of the collisional moments μ_4 and μ_6 for $\zeta_0 = 1$, $\gamma = 0.1$, $d = 3$, and initial conditions $a_2^0 = 0.5$ and (a, b) $\theta^0 = 10$, (c, d) $\theta^0 = 3.15$, (e, f) $\theta^0 = 2$, (g, h) $\theta^0 = 1.5$, (i, j) $\theta^0 = 1.05$, (k, l) $\theta^0 = 1.01$, and (m, n) $\theta^0 = 0.91$. Symbols correspond to simulation data for DSMC (\circ) and EDMD (\times) schemes, while lines represent the theoretical predictions for ESA (—) and BSA (\cdots).

in Eq. (C2), and $\bar{\mathbf{Y}}_i$ is an independent random vector, also drawn from the Gaussian distribution (C3). Notice that, since the equation for $\mathbf{v}_i(t)$ is expanded up to $\mathcal{O}(h^{3/2})$ and $\mathbf{r}_i(t+h) - \mathbf{r}_i(t) \sim \mathbf{v}_i(t)h$, then the equation for $\mathbf{r}_i(t)$ needs to be expanded up to $\mathcal{O}(h^{5/2})$.

In our EDMD simulations, we deal with a system of $N = 1.065 \times 10^4$ spheres and reduced number density $n\sigma^3 = 10^{-3}$. The time step is $h = 10^{-3}\lambda/\sqrt{2k_B T_b/m}$, and periodic boundary conditions are used.

3. Test of the time evolution of the collisional moments μ_4 and μ_6

Let us present now a comparison between the collisional moments μ_4 and μ_6 measured in simulations and those provided by the ESA and the BSA. In the ESA, those collisional moments are given by Eqs. (31), complemented with the numerical solution of Eqs. (21) and (32). Analogously, in the BSA, the collisional moments are given by Eqs. (31) with $a_3 \rightarrow 0$, complemented with

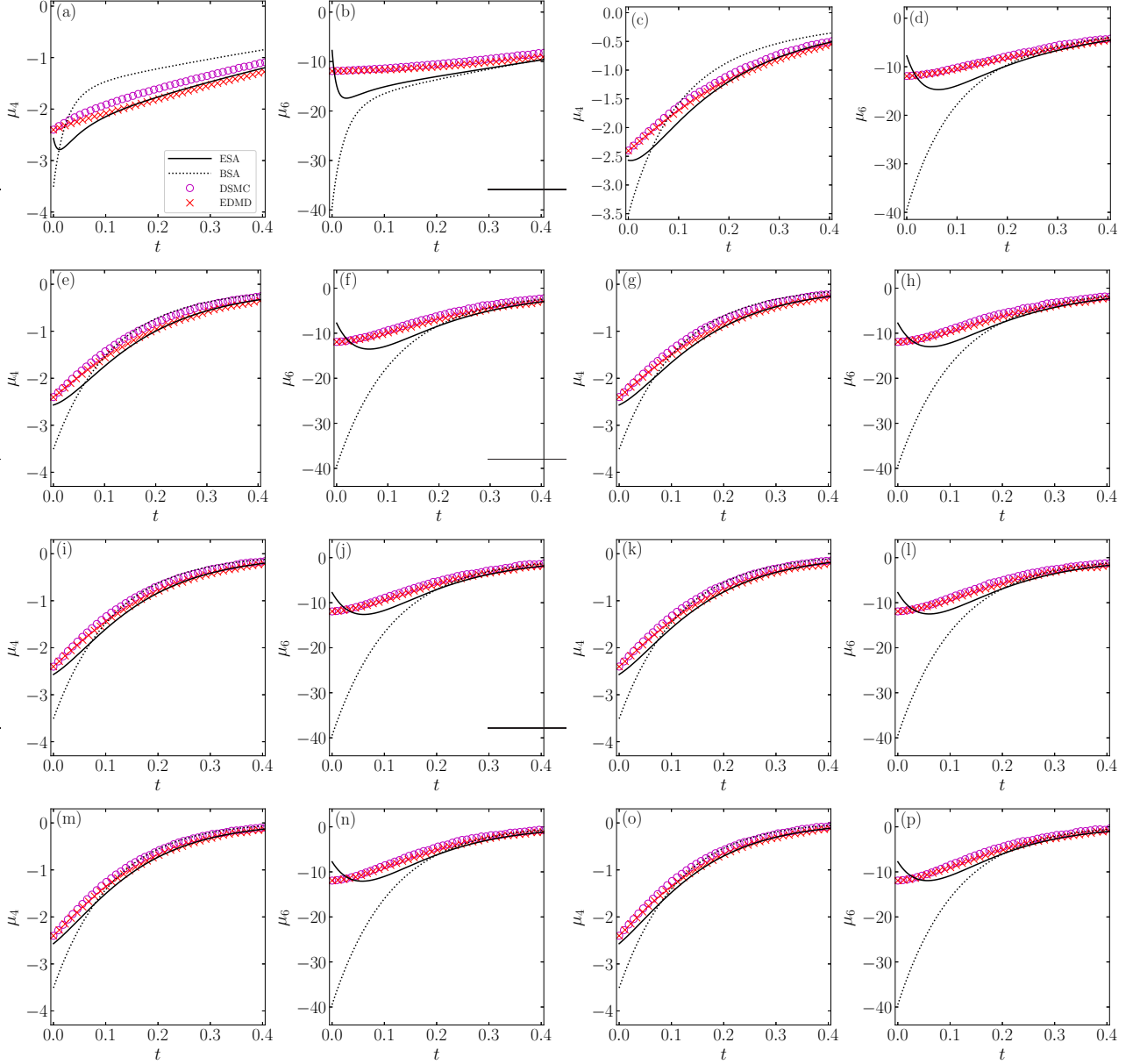


FIG. 14. Evolution of the collisional moments μ_4 and μ_6 for $\zeta_0 = 1$, $\gamma = 0.1$, $d = 3$, and initial conditions $a_2^0 = -0.35$ and (a, b) $\theta^0 = 9$, (c, d) $\theta^0 = 1.8$, (e, f) $\theta^0 = 1.27$, (g, h) $\theta^0 = 1.1$, and (i, j) $\theta^0 = 0.99$, (k, l) $\theta^0 = 0.96$, (m, n) $\theta^0 = 0.85$, and (o, p) $\theta^0 = 0.82$. Symbols correspond to simulation data for DSMC (\circ) and EDMD (\times) schemes, while lines represent the theoretical predictions for ESA (—) and BSA (\cdots).

the numerical solution of Eqs. (21) and (32a), again with $a_3 \rightarrow 0$.

In the simulations (both DSMC and EDMD), the following numerical scheme has been used to address the computation of the collisional moments [96, 98]. We randomly choose $N' = 10^6$ pairs of particles out of the total number $N(N-1)/2 = 5 \times 10^7$ and approximate the collisional moments as

$$\mu_\ell = \frac{1}{N'} \sum_{ij}^{N'} \Phi_\ell(\mathbf{c}_i, \mathbf{c}_j), \quad (\text{C6})$$

where Φ_4 and Φ_6 are given by Eqs. (26).

Figures 13 and 14 show the time evolution of μ_4 and μ_6 , as measured in our DSMC and EDMD simulations and as predicted by the BSA and ESA, for a number of representative initial conditions. A very good agreement between DSMC and EDMD is found; the small differences between them could explain the deviations observed in Figs. 8–10. There is also a general good agreement with the ESA results, while the BSA predictions exhibit important deviations in the initial stage, especially in the case of μ_6 . The deviations of the BSA and ESA are due

to the nonnegligible role played by nonlinear terms of the form a_2^2 , a_3^2 , and a_2a_3 , as well as by higher-order cumulants. Interestingly, those deviations are more relevant for negative a_2^0 than for positive a_2^0 and tend to increase as the initial temperature θ^0 grows—in accordance with the results in Ref. [37] for a quench to low temperatures.

Appendix D: Evolution of the cumulants a_2 and a_3

In this Appendix we present a comparison between the simulation results for the cumulants a_2 and the theoretical predictions BSA (for a_2 only) and ESA. The results are displayed in Figs. 15–18.

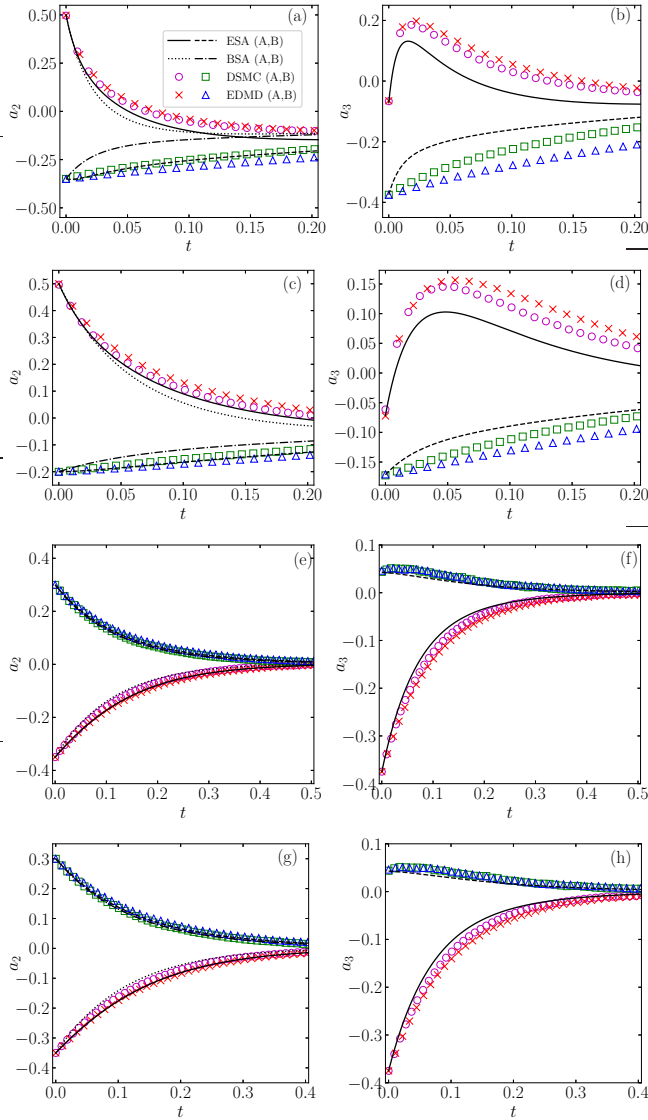


FIG. 15. Same as in Fig. 9, except that the quantities plotted are a_2 and a_3 .

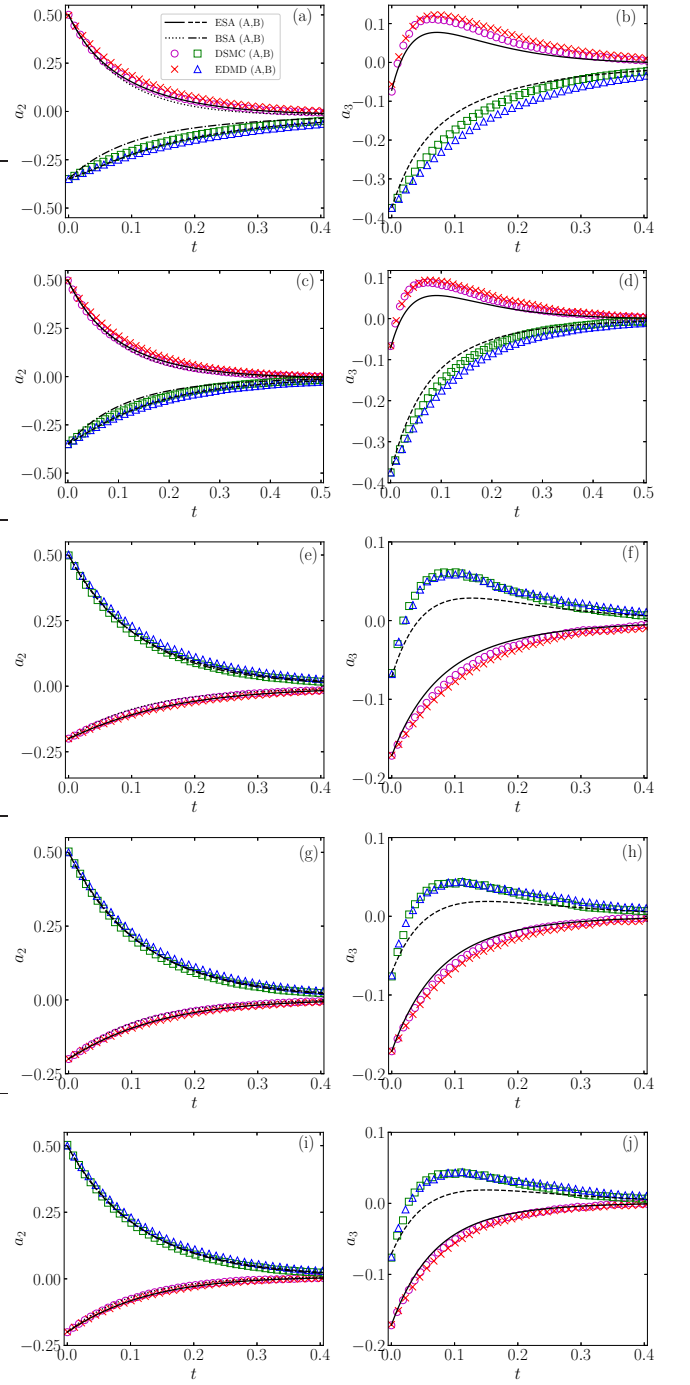


FIG. 16. Same as in Fig. 10, except that the quantities plotted are a_2 and a_3 .

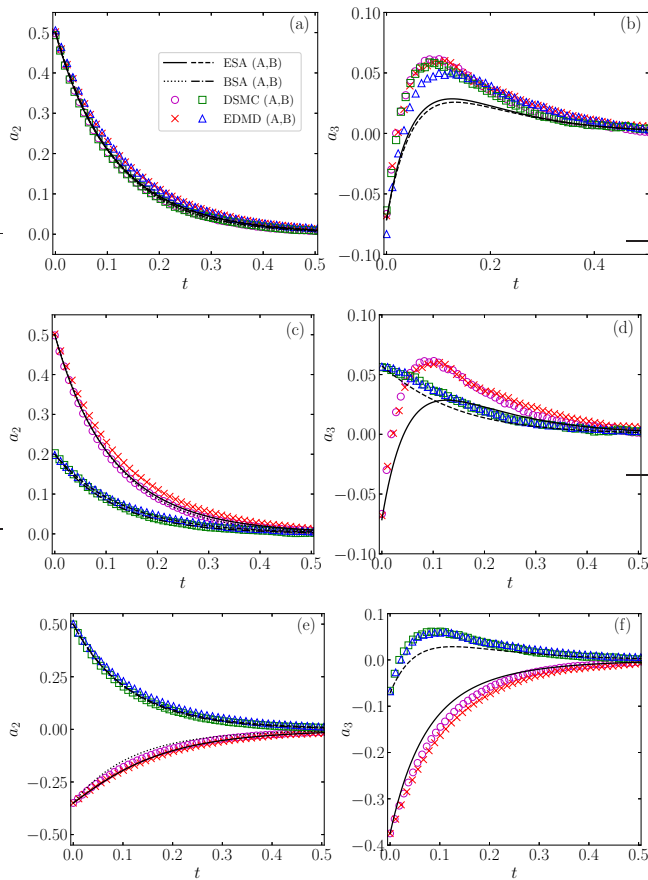


FIG. 17. Same as in Fig. 11, except that the quantities plotted are a_2 and a_3 .

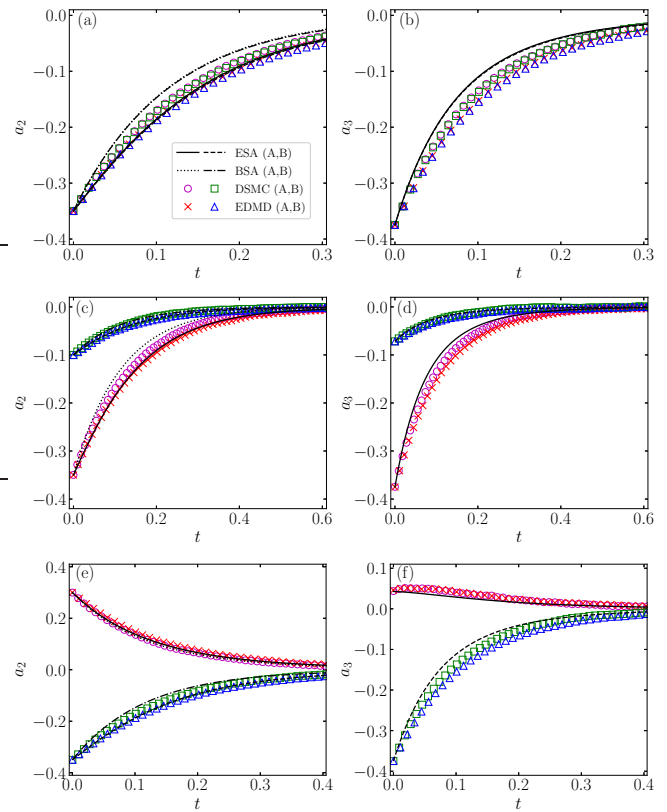


FIG. 18. Same as in Fig. 12, except that the quantities plotted are a_2 and a_3 .

-
- [1] N. C. Keim, J. D. Paulsen, Z. Zeravcic, S. Sastry, and S. R. Nagel, Memory formation in matter, *Rev. Mod. Phys.* **91**, 035002 (2019).
- [2] E. B. Mpemba and D. G. Osborne, Cool?, *Phys. Educ.* **4**, 172 (1969).
- [3] G. S. Kell, The freezing of hot and cold water, *Am. J. Phys.* **37**, 564 (1969).
- [4] I. Firth, Cooler?, *Phys. Educ.* **6**, 32 (1971).
- [5] E. Deeson, Cooler-lower down, *Phys. Educ.* **6**, 42 (1971).
- [6] F. C. Frank, The Descartes–Mpemba phenomenon, *Phys. Educ.* **9**, 284 (1974).
- [7] R. Gallea, The Bacon–Descartes–Mpemba phenomenon, *Phys. Educ.* **9**, 490 (1974).
- [8] J. Walker, Hot water freezes faster than cold water. Why does it do so?, *Sci. Am.* **237**, 246 (1977).
- [9] D. G. Osborne, Mind on ice, *Phys. Educ.* **14**, 414 (1979).
- [10] M. Freeman, Cooler still — an answer?, *Phys. Educ.* **14**, 417 (1979).
- [11] K. Kumar, Mpemba effect and 18th century ice-cream, *Phys. Educ.* **15**, 268 (1980).
- [12] J. W. Hanneken, Mpemba effect and cooling by radiation to the sky, *Phys. Educ.* **16**, 7 (1981).
- [13] B. Wojciechowski, I. Owczarek, and G. Bednarz, Freezing of aqueous solutions containing gases, *Cryst. Res. Technol.* **23**, 843 (1988).
- [14] D. Auerbach, Supercooling and the Mpemba effect: When hot water freezes quicker than cold, *Am. J. Phys.* **63**, 882 (1995).
- [15] C. A. Knight, The Mpemba effect: The freezing times of cold and hot water, *Am. J. Phys.* **64**, 524 (1996).
- [16] P. K. Maciejewski, Evidence of a convective instability allowing warm water to freeze in less time than cold water, *J. Heat Transf.* **118**, 65 (1996).
- [17] M. Jeng, The Mpemba effect: When can hot water freeze faster than cold?, *Am. J. Phys.* **74**, 514 (2006).
- [18] S. Esposito, R. De Risi, and L. Somma, Mpemba effect and phase transitions in the adiabatic cooling of water before freezing, *Physica A* **387**, 757 (2008).
- [19] J. I. Katz, When hot water freezes before cold, *Am. J. Phys.* **77**, 27 (2009).
- [20] M. Vynnycky and S. L. Mitchell, Evaporative cooling and the Mpemba effect, *Heat Mass Transf.* **46**, 881 (2010).
- [21] J. D. Brownridge, When does hot water freeze faster than cold water? A search for the Mpemba effect, *Am. J. Phys.* **79**, 78 (2011).
- [22] M. Vynnycky and N. Maeno, Axisymmetric natural convection-driven evaporation of hot water and the Mpemba effect,

- Int. J. Heat Mass Transf. **55**, 7297 (2012).
- [23] M. Balázovič and B. Tomášik, The Mpemba effect, Shechtman’s quasicrystals and student exploration activities, *Phys. Educ.* **47**, 568 (2012).
- [24] X. Zhang, Y. Huang, Z. Ma, Y. Zhou, J. Zhou, W. Zheng, Q. Jiang, and C. Q. Sun, Hydrogen-bond memory and water-skin supersolidity resolving the Mpemba paradox, *Phys. Chem. Chem. Phys.* **16**, 22995 (2014).
- [25] M. Vynnycky and S. Kimura, Can natural convection alone explain the Mpemba effect?, *Int. J. Heat Mass Transf.* **80**, 243 (2015).
- [26] C. Q. Sun, Behind the Mpemba paradox, *Temperature* **2**, 38 (2015).
- [27] M. Balázovič and B. Tomášik, Paradox of temperature decreasing without unique explanation, *Temperature* **2**, 61 (2015).
- [28] A. A. Romanovsky, Which is the correct answer to the Mpemba puzzle?, *Temperature* **2**, 63 (2015).
- [29] J. Jin and W. A. Goddard, Mechanisms underlying the Mpemba effect in water from molecular dynamics simulations, *J. Phys. Chem. C* **119**, 2622 (2015).
- [30] R. T. Ibekwe and J. P. Cullerne, Investigating the Mpemba effect: when hot water freezes faster than cold water, *Phys. Educ.* **51**, 025011 (2016).
- [31] A. Gijón, A. Lasanta, and E. R. Hernández, Paths towards equilibrium in molecular systems: The case of water, *Phys. Rev. E* **100**, 032103 (2019).
- [32] J. Bechhoefer, A. Kumar, and R. Chétrite, A fresh understanding of the Mpemba effect, *Nat. Rev. Phys.* **3**, 534 (2021).
- [33] H. C. Burridge and P. F. Linden, Questioning the Mpemba effect: hot water does not cool more quickly than cold, *Sci. Rep.* **6**, 37665 (2016).
- [34] H. C. Burridge and O. Hallstadius, Observing the Mpemba effect with minimal bias and the value of the Mpemba effect to scientific outreach and engagement, *Proc. R. Soc. A* **476**, 20190829 (2020).
- [35] D. C. Elton and P. D. Spencer, Pathological Water Science — Four Examples and What They Have in Common, in *Biomechanical and Related Systems*, Biologically-Inspired Systems, Vol. 17, edited by A. Gadomski (Springer, Cham., 2021) pp. 155–169.
- [36] A. Santos and A. Prados, Mpemba effect in molecular gases under nonlinear drag, *Phys. Fluids* **32**, 072010 (2020).
- [37] A. Patrón, B. Sánchez-Rey, and A. Prados, Strong non-exponential relaxation and memory effects in a fluid with nonlinear drag, *Phys. Rev. E* **104**, 064127 (2021).
- [38] R. Gómez González, N. Khalil, and V. Garzó, Mpemba-like effect in driven binary mixtures, *Phys. Fluids* **33**, 053301 (2021).
- [39] A. Lasanta, F. Vega Reyes, A. Prados, and A. Santos, When the hotter cools more quickly: Mpemba effect in granular fluids, *Phys. Rev. Lett.* **119**, 148001 (2017).
- [40] A. Torrente, M. A. López-Castaño, A. Lasanta, F. Vega Reyes, A. Prados, and A. Santos, Large Mpemba-like effect in a gas of inelastic rough hard spheres, *Phys. Rev. E* **99**, 060901(R) (2019).
- [41] A. Biswas, V. V. Prasad, O. Raz, and R. Rajesh, Mpemba effect in driven granular Maxwell gases, *Phys. Rev. E* **102**, 012906 (2020).
- [42] E. Mompó, M. A. López Castaño, A. Torrente, F. Vega Reyes, and A. Lasanta, Memory effects in a gas of viscoelastic particles, *Phys. Fluids* **33**, 062005 (2021).
- [43] R. Gómez González and V. Garzó, Time-dependent homogeneous states of binary granular suspensions, *Phys. Fluids* **33**, 093315 (2021).
- [44] A. Biswas, V. V. Prasad, and R. Rajesh, Mpemba effect in an anisotropically driven granular gas, *EPL* **XX**, YY (2021).
- [45] S. Takada, H. Hayakawa, and A. Santos, Mpemba effect in inertial suspensions, *Phys. Rev. E* **103**, 032901 (2021).
- [46] S. Takada, Homogeneous cooling and heating states of dilute soft-core gases under nonlinear drag, *EPJ Web Conf.* **249**, 04001 (2021).
- [47] M. Baity-Jesi, E. Calore, A. Cruz, L. A. Fernandez, J. M. Gil-Narvión, A. Gordillo-Guerrero, D. Iñiguez, A. Lasanta, A. Maiorano, E. Marinari, V. Martin-Mayor, J. Moreno-Gordo, A. Muñoz-Sudupe, D. Navarro, G. Parisi, S. Perez-Gavero, F. Ricci-Tersenghi, J. J. Ruiz-Lorenzo, S. F. Schifano, B. Seoane, A. Tarancón, R. Tripiccion, and D. Yllanes, The Mpemba effect in spin glasses is a persistent memory effect, *Proc. Natl. Acad. Sci. U. S. A.* **116**, 15350 (2019).
- [48] P. A. Greaney, G. Lani, G. Cicero, and J. C. Grossman, Mpemba-like behavior in carbon nanotube resonators, *Metall. Mater. Trans. A* **42**, 3907 (2011).
- [49] Y.-H. Ahn, H. Kang, D.-Y. Koh, and H. Lee, Experimental verifications of Mpemba-like behaviors of clathrate hydrates, *Korean J. Chem. Eng.* **33**, 1903 (2016).
- [50] Z. Lu and O. Raz, Nonequilibrium thermodynamics of the Markovian Mpemba effect and its inverse, *Proc. Natl. Acad. Sci. U. S. A.* **114**, 5083 (2017).
- [51] I. Klich, O. Raz, O. Hirschberg, and M. Vucelja, Mpemba index and anomalous relaxation, *Phys. Rev. X* **9**, 021060 (2019).
- [52] R. Chétrite, A. Kumar, and J. Bechhoefer, The metastable Mpemba effect corresponds to a non-monotonic temperature dependence of extractable work, *Front. Physics* **9**, 654271 (2021).
- [53] D. M. Busiello, D. Gupta, and A. Maritan, Inducing and optimizing Markovian Mpemba effect with stochastic reset, *New J. Phys.* **23**, 103012 (2021).
- [54] J. Lin, K. Li, J. He, J. Ren, and J. Wang, Power statistics of Otto heat engines with the Mpemba effect, *Phys. Rev. E* **105**, 014104 (2022).
- [55] F. J. Schwarzendahl and H. Löwen, Anomalous cooling and overcooling of active systems, *arXiv:2111.06109* (2021).
- [56] I. González-Adalid Pemartín, E. Mompó, A. Lasanta, V. Martín-Mayor, and J. Salas, Slow growth of magnetic domains helps fast evolution routes for out-of-equilibrium dynamics, *Phys. Rev. E* **104**, 044114 (2021).
- [57] G. Teza, R. Yaacoby, and O. Raz, Relaxation shortcuts through boundary coupling, *arXiv:2112.10187* (2021).
- [58] Z.-Y. Yang and J.-X. Hou, Non-Markovian Mpemba effect in mean-field systems, *Phys. Rev. E* **101**, 052106 (2020).
- [59] Z.-Y. Yang and J.-X. Hou, Mpemba effect of a mean-field system: The phase transition time, *Phys. Rev. E* **105**, 014119 (2022).
- [60] F. Carollo, A. Lasanta, and I. Lesanovsky, Exponentially accelerated approach to stationarity in Markovian open quantum systems through the Mpemba effect, *Phys. Rev. Lett.* **127**, 060401 (2021).
- [61] A. Kumar and J. Bechhoefer, Exponentially faster cooling in a colloidal system, *Nature* **584**, 64 (2020).

- [62] A. Kumar, R. Chérite, and J. Bechhoefer, Anomalous heating in a colloidal system, *Proc. Natl. Acad. Sci. U. S. A.* **119**, e2118484119 (2022).
- [63] S. Kullback and R. A. Leibler, On information and sufficiency, *Ann. Math. Statist.* **22**, 79 (1951).
- [64] N. G. V. Kampen, *Stochastic Processes in Physics and Chemistry* (North-Holland, Amsterdam, 2007).
- [65] Strictly speaking, the KLD does not have the properties of a distance; e.g., it does not satisfy the triangle inequality.
- [66] L. Ferrari, Particles dispersed in a dilute gas: Limits of validity of the Langevin equation, *Chem. Phys.* **336**, 27 (2007).
- [67] L. Ferrari, Particles dispersed in a dilute gas. II. From the Langevin equation to a more general kinetic approach, *Chem. Phys.* **428**, 144 (2014).
- [68] M. Hohmann, F. Kindermann, T. Lausch, D. Mayer, F. Schmidt, E. Lutz, and A. Widera, Individual tracer atoms in an ultracold dilute gas, *Phys. Rev. Lett.* **118**, 263401 (2017).
- [69] J. R. Dorfman and H. van Beijeren, The kinetic theory of gases, in *Statistical Mechanics, Part B*, edited by B. Berne (Plenum, New York, 1977) pp. 65–179.
- [70] Note that, because of the second equality in Eq. (12b), the entropic “distance” \mathcal{D} from f to f^{LE} is exactly given by the distance from f to f^{LE} plus the distance from f^{LE} to f^{eq} . The decomposition (11) can be schematically depicted as
- $$\underbrace{f(\mathbf{v}, t) \longrightarrow f^{\text{LE}}(\mathbf{v}; T(t))}_{\mathcal{D}^{\text{kin}}(t)} \xrightarrow{\mathcal{D}(t)} \underbrace{f^{\text{LE}}(\mathbf{v}; T(t)) \longrightarrow f^{\text{eq}}(\mathbf{v})}_{\mathcal{D}^{\text{LE}}(T(t))}.$$
- [71] T. R. Kirkpatrick, D. Belitz, and J. R. Dorfman, Nonhydrodynamic initial conditions are not soon forgotten, *Phys. Rev. E* **104**, 024111 (2021).
- [72] In that case, $\tau_b \rightarrow \infty$ and one has to change the definition of dimensionless time to $\zeta_0 t$.
- [73] M. Jauregui, A. L. F. Lucchi, J. H. Y. Passos, and R. S. Mendes, Stationary solution and h theorem for a generalized Fokker-Planck equation, *Phys. Rev. E* **104**, 034130 (2021).
- [74] N. Brilliantov and T. Pöschel, Breakdown of the Sonine expansion for the velocity distribution of granular gases, *Europhys. Lett.* **74**, 424 (2006), Erratum: **75**, 188 (2006).
- [75] This was the approach carried out in a previous work to analyze the TME [36].
- [76] This approximation has been employed in Ref. [37] to study the response of the nonlinear fluid to a low-temperature quench.
- [77] For the EME, there is not a clear cut distinction between the direct and inverse EME (since the relative entropy \mathcal{D} is positive definite), unless the initial temperatures are known.
- [78] R. V. Hogg and A. T. Craig, *Introduction to Mathematical Statistics*, 4th ed. (Macmillan Publishing, New York, 1978) pp. 103–108.
- [79] W. D. Penny, KL-Divergences of Normal, Gamma, Dirichlet, and Wishart densities, www.fil.ion.ucl.ac.uk/~wpenny/publications/densities.ps.
- [80] M. Abramowitz and I. A. Stegun, eds., *Handbook of Mathematical Functions* (Dover, New York, 1972).
- [81] A. J. Kovacs, Transition vitreuse dans les polymères amorphes. Etude phénoménologique, *Fortschr. Hochpolym.-Forsch.* **3**, 394 (1963).
- [82] A. J. Kovacs, J. J. Aklonis, J. M. Hutchinson, and A. R. Ramos, Isobaric volume and enthalpy recovery of glasses. II. A transparent multiparameter theory, *J. Polym. Sci. Pol. Phys.* **17**, 1097 (1979).
- [83] A. Prados and J. J. Brey, The Kovacs effect: a master equation analysis, *J. Stat. Mech.*, P02009 (2010).
- [84] E. Bouchbinder and J. S. Langer, Nonequilibrium thermodynamics of the Kovacs effect, *Soft Matter* **6**, 3065 (2010).
- [85] A. Prados and E. Trizac, Kovacs-like memory effect in driven granular gases, *Phys. Rev. Lett.* **112**, 198001 (2014).
- [86] E. Trizac and A. Prados, Memory effect in uniformly heated granular gases, *Phys. Rev. E* **90**, 012204 (2014).
- [87] A. Lasanta, F. Vega Reyes, A. Prados, and A. Santos, On the emergence of large and complex memory effects in nonequilibrium fluids, *New J. Phys.* **21**, 033042 (2019).
- [88] A. Megías and A. Santos, Kullback–Leibler divergence of a freely cooling granular gas, *Entropy* **22**, 1308 (2020).
- [89] A. Megías and A. Santos, Relative entropy of freely cooling granular gases. a molecular dynamics study, *EPJ Web Conf.* **249**, 04006 (2021).
- [90] A. Lapolla and A. Godec, Faster uphill relaxation in thermodynamically equidistant temperature quenches, *Phys. Rev. Lett.* **125**, 110602 (2021).
- [91] T. Van Vu and Y. Hasegawa, Toward relaxation asymmetry: Heating is faster than cooling, *Phys. Rev. Res.* **3**, 043160 (2021).
- [92] R. Mannella and P. V. E. McClintock, Itô versus Stratonovich: 30 years later, *Fluct. Noise Lett.* **11**, 1240010 (2012).
- [93] Y. L. Klimontovich, Nonlinear Brownian motion, *Physics-Uspekhi* **37**, 737 (1994).
- [94] G. A. Bird, *Molecular Gas Dynamics and the Direct Simulation of Gas Flows* (Clarendon, Oxford, UK, 1994).
- [95] G. A. Bird, *The DSMC Method* (CreateSpace Independent Publishing Platform, 2013).
- [96] J. M. Montanero and A. Santos, Computer simulation of uniformly heated granular fluids, *Granul. Matter* **2**, 53 (2000).
- [97] A. Scala, Event-driven Langevin simulations of hard spheres, *Phys. Rev. E* **86**, 026709 (2012).
- [98] A. Santos and J. M. Montanero, The second and third Sonine coefficients of a freely cooling granular gas revisited, *Granul. Matter* **11**, 157 (2009).